Novel Designs for Photovoltaic Arrays to Reduce Partial Shading Losses and to Ease Series Arc Fault Detection

by

Mohamed Zakaria Mohamed Ahmed Shams El-Dein

A thesis
presented to the University of Waterloo
in fulfilment of the
thesis requirement for the degree of
Doctor of Philosophy
in
Electrical and Computer Engineering

Waterloo, Ontario, Canada, 2012

Author’s Declaration

I hereby declare that I am the sole author of this thesis. This is a true copy of the thesis, including any required final revisions, as accepted by my examiners.

I understand that my thesis may be made electronically available to the public.

Abstract

A mismatch in a photovoltaic array implies differences in the I-V characteristics of the modules forming the array which can lead to significant energy losses known as mismatch losses. The sources of mismatch losses could be easy- or difficult-to-predict sources. This thesis proposes novel designs for photovoltaic arrays to reduce mismatch losses.

The mismatch from easy-to-predict sources and its resulting losses can be reduced by altering the interconnection of the array. Therefore, this thesis proposes an optimal total-cross-tied interconnection, based on a thorough mathematical formulation, which can significantly reduce mismatch losses from easy-to-predict sources. Application examples of the operation of the optimal total-cross-tied interconnection under partial shading are presented.

The effect of partial shading caused by easy- or difficult-to-predict sources can be considerably reduced by photovoltaic array reconfiguration. This thesis proposes a novel mathematical formulation for the optimal reconfiguration of photovoltaic arrays to minimize partial shading losses. The thesis formulates the reconfiguration problem as a mixed integer quadratic programming problem and finds the optimal solution using branch-and-bound algorithm. The proposed formulation can be used for equal or non-equal number of modules per row. Moreover, it can be used for fully reconfigurable or partially-reconfigurable arrays. Application examples of the operation of the reconfigurable photovoltaic array under partial shading are presented.

Finally, the recently updated American National Electric Code requires the presence of a series arc fault detector in any Photovoltaic installation operating at a voltage greater than or equal to 80V. However, the Photovoltaic market nowadays lacks the presence of an accurate series arc fault detector that can detect series arc faults and discriminate between them and partial shading. The work in this thesis proposes an algorithm that can detect series arc faults and discriminate between them and partial shading in total-cross-tied arrays. This algorithm is based on the measurement of instantaneous row voltages.

Acknowledgements

Thank God for helping me to achieve this work.

I then would like to thank my supervisors, Professor Mehrdad Kazerani and Professor Magdy Salama for their continuous guidance throughout the period of my PhD studies. Their valuable suggestions and discussions were always helpful and inspiring. Also, their support and encouragement were my greatest motive to aim for the best.

I would also like to thank my Ph.D. committee members: Professor Tarek Abdel-Galil, Professor Ehab El-Saadany, Professor Samir El-Hedhli, and the external examiner Professor Luiz Lopes from the University of Concordia.

Also, many thanks to my colleagues in the power group for their help and support.

I would like to show my deepest gratitude and respect to my family, especially my parents, the ones to whom I owe all the success in my life. No words can express my gratitude to them, but I pray God to bless them and reward them.

A final word to my wife; without you I could have never been able to achieve this work. Your patience and encouragement were always a source of strength for me. You are the shining moon that lightens my life.

Table of Contents

List of Figures

List of Tables

List of Acronyms

a	Switch Cost ($)
b	Current Sensor
BL	Bridge Linked
c	Voltage sensor cost ($)
CE	Negotiated Contract Price ($)
CPV	Cost Present Value ($)
d	Controller Cost ($)
D	Discount Rate
EA	Annual array's energy production under mismatch (Wh)
EA_{max}	Annual array's maximum energy during mismatch (Wh)
F	Inflation Rate
FRPVA	Full Reconfigurable PhotoVoltaic Array
G	Reference irradiance level (W/m^2)
g	Time segment index
HA	Annual array's in plane irradiance level during mismatch (Wh/m^2)
HC	Honey Comb
i	Row index
IA_g	Array's current at time segment *g* (A)
IRR_{qg}	Module q irradiance level at time segment *g* (W/m^2)
$IRRA_g$	Arrays' irradiance level at time segment g (W/m^2)
I_{oq}	Module q reverse bias diode saturation current (A)
IM_{qg}	Module q current at time segment *g* (A)
I_{scq}	Module q short circuit current at reference irradiance level (A)
IMI	Irradiance level mismatch index
IRA	Arrays' total irradiance level (W/m^2)
IRF_i	Irradiance level of the fixed part of row i (W/m^2)
IRM_q	Irradiance level of the reconfigurable module q (W/m^2)
IRR_i	Total irradiance level of row i (W/m^2)
j	Columns index
l	Row index

M	Total number of rows
$MPPA_g$	Array's maximum power point at time segment g (kW)
MPPT	Maximum Power Point Tracker
N	Total number of columns
n_F	Number of fixed columns
n_R	Number of reconfigurable columns
N	Total number of mismatch situations
N_I	Number of current sensors
N_V	Number of voltage sensors
N_{sh}	The number of the partially shaded rows
N_{sq}	Module q total number of series modules
N_{sw}	Number of Switches
NNZ	Number of None Zero elements during partial shading
NPV	Net Present Value ($)
P_{dc}	Array's dc rating (kW)
PA	Array's output power (W)
PR	Performance Ratio
PS	Partial Shading
Q	Module index
RPV	Revenue Present Value ($)
R_{sq}	Module q series resistance (Ω)
R_{Pq}	Module q parallel resistance (Ω)
$RVMI_{il}$	Row Voltage Mismatch Index between row i and row l (V^2)
SP	Series Parallel
t_g	Time duration of time segment *g* (hr)
T	Optimization processing time (s)
TCT	Total Cross Tied
VA_g	Array's voltage at time segment *g* (V)
VR_{ig}	Row i voltage at time segment *g* (V)
VM_{qg}	Module q voltage at time segment *g* (V)
V_{Tq}	Module q thermal voltage (V)
Y	Array life time (years)

y_{ijq} Existence variable for optimal total cross tied interconnection

y_{iq} Existence variable for optimal photovoltaic array reconfiguration

Chapter 1
Introduction

1.1 Preface

Energy production from renewable energy sources is accelerating due to the increase in oil prices, depletion of fossil fuel reservoirs, energy security concerns, worries about climate change and public health concerns. Known Renewable energy sources include hydro, wind, tidal, geothermal, bio, and solar. The energy received from solar irradiation in the form of light can be directly converted to electricity through PhotoVoltaic (PV) process. Photovoltaic conversion does not produce any harmful byproducts; it is renewable and clean. Also, it does not have any moving parts, which makes it an attractive solution from the maintenance requirements and life span points of view.

PV power systems offer a variety of applications, ranging from a few miliwatts to tens of megawatts. These applications could be non-terrestrial or terrestrial. Non-terrestrial applications are like calculators, mobiles and satellites, while terrestrial applications are like buildings, pumps and telecommunication antennas. Terrestrial applications are divided into stand-alone systems—which are not connected to the electrical utility grid—and utility grid-connected systems. Stand-alone systems could be subdivided into domestic applications like households and villages and non-domestic applications like telecommunications, pumps and navigational aids. Also, utility-connected systems could be subdivided into residential, intermediate and central station [1]. The residential and intermediate are treated as Distributed Generation (DG) and the central station is treated as a power plant. Figure 1-1 shows PV applications classification. The focus of this thesis is on terrestrial applications, although the results could be applied to other applications as well.

In the year 2010, about 15 GW of new terrestrial PV was installed in International Energy Agency (IEA) Countries, showing about 75 % increase over the installed capacity in 2009. These new installations increased the total installed capacity in IEA countries to about 35 GW at the end of 2010 [2]. Figure 1-2 shows the total installed capacity of terrestrial PV power in IEA countries. Canada's installed capacity reached 300 MW at the end of 2010, making Canada one of the top ten IEA countries in installing PV [2]. In Ontario, there is a great incentive for investing in PV through Ontario's Feed-In Tariff (FIT) Program, which is a pricing structure for renewable electricity production. This program pays from 44.3 to 80.2 ¢/kWh for the electricity generated from solar energy and from 13.5 to 19 ¢/kWh for electricity generated from wind energy [3]. This incentive

motivated companies like First Solar and Enbridge to build the largest PV farm in the world of 80 MW capacities in Sarnia, Ontario [4].

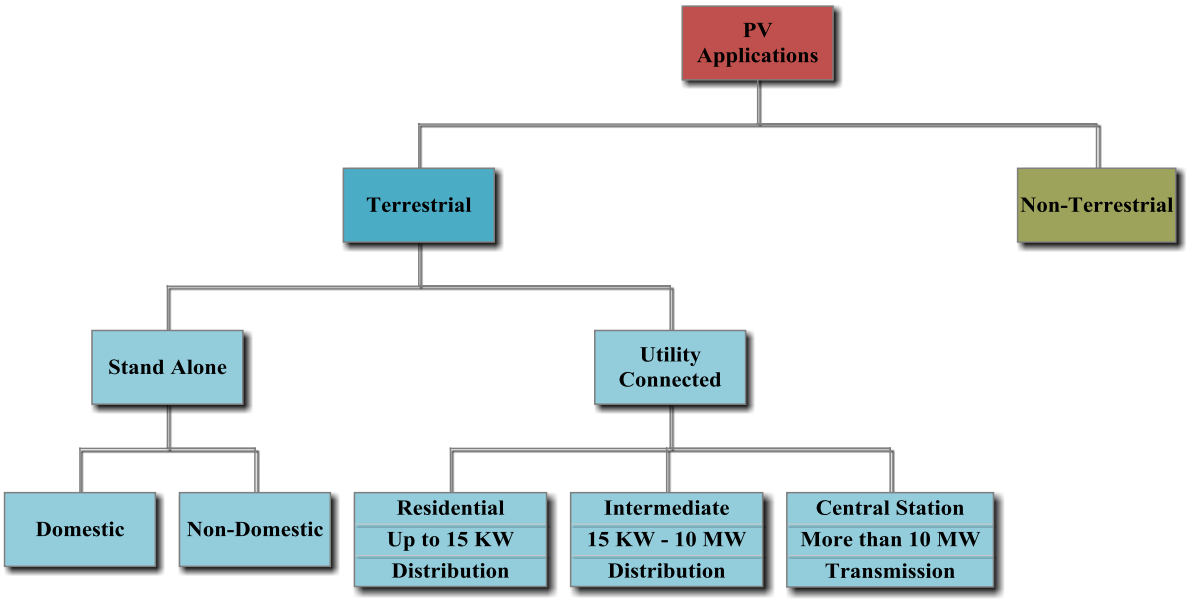

Figure 1-1: PV applications

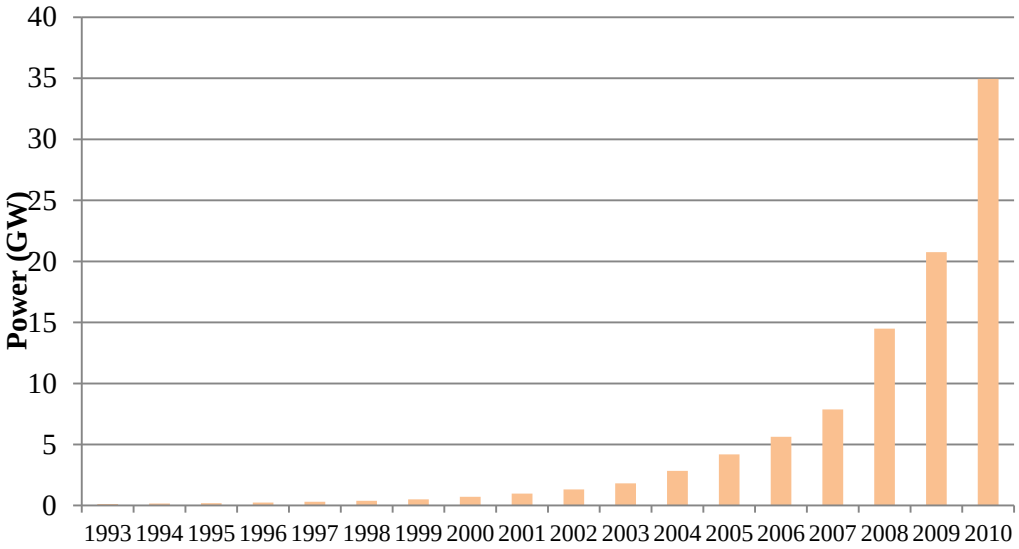

Figure 1-2: Cumulative installed terrestrial PV power in IEA countries

1.2 Motivation

The use of PV systems for power generation brings many challenges. For example, neighboring buildings, trees, arrays, snow, soiling or passing clouds can cause PV arrays to be partially shaded. Moreover, loose connections, animal bits or bad installation can cause series arc faults in PV arrays. The following points are the motivations behind this thesis.

1. In Building-Integrated PhotoVoltaic (BIPV), partial shading causes an annual energy loss of 5-10 % [2-3], [70], as reported in Germany, Japan and USA.

2. In PV farms, partial shading causes an annual energy loss of 2-7 % [4], [71], as reported in Spain. Figure 1-3 shows partial shading in a PV farm in California due to dust and Figures 1-4 and 1-5 show partial shading in Sarnia PV farm due to clouds and snow. In addition to annual energy losses, PV farms are usually installed over large areas to avoid partial shading caused by consecutive rows, as shown in Figure 1-6, thus increasing the land cost. Moreover, PV arrays are usually installed in landscape installation with reduced number of rows to avoid partial shading losses which increases the installation cost when compared to portrait installation, shown in Figure 1-7, and high number of rows, shown in Figure 1-8.

3. Series arc faults cause fire, severe damage and profit loss to PV systems, as reported in many countries around the world [5-8] and shown in Figure 1-9. Therefore, the 2011 National American Electrical Code requires series arc fault detection in any PV systems operating at a voltage greater than or equal to 80 V.

Figure 1-3: Dust partial shading in California PV farm

Figure 1-4: Clouds partial shading in Sarnia PV farm

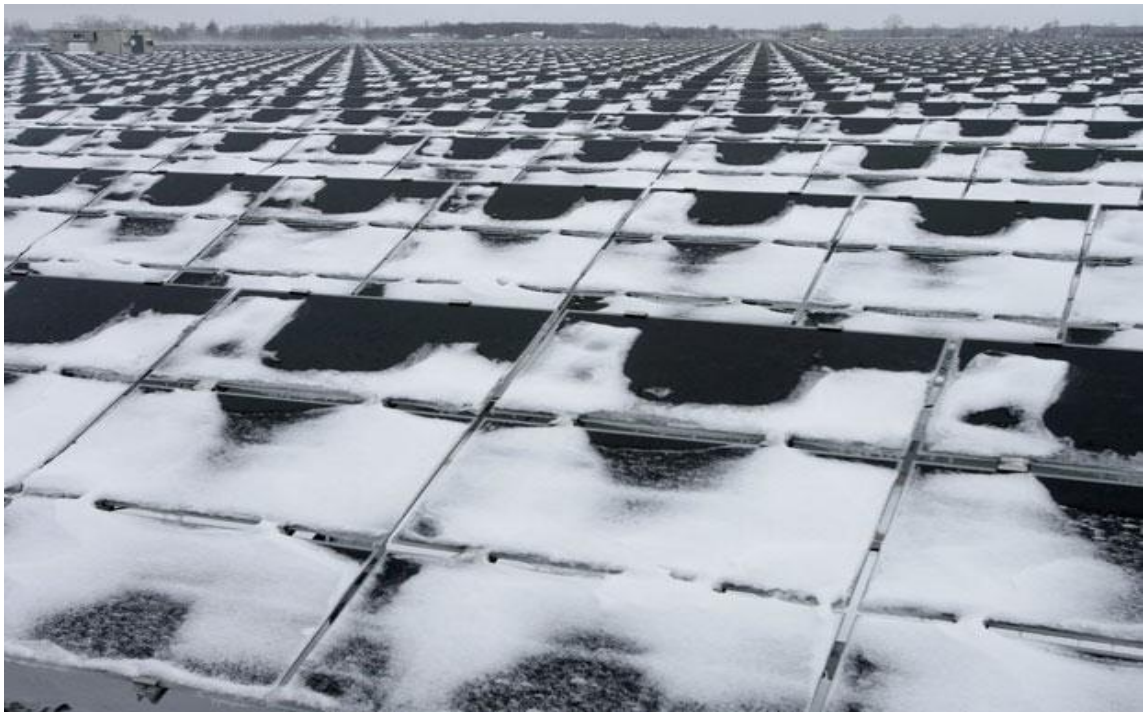

Figure 1-5: Snow partial shading in Sarnia PV farm

Figure 1-6: Sarnia PV farm is installed on a large area and in landscape to avoid array partial shading

Figure 1-7: A PV farm installed in portrait to reduce installation cost

Figure 1-8: A PV array which large number of rows to reduce installation cost

Figure 1-9: A PV farm fire and damage due to series arc fault

1.3 Thesis Objectives

The main focus of the thesis is to develop new designs for PV arrays to overcome partial shading and series arc fault problems. The objectives of this thesis are as follows:

1. Finding the optimal interconnection of PV modules in a PV array to reduce partial shading losses caused by easy-to-predict sources such as nearby arrays and buildings;
2. Finding the optimal PV module reconfiguration to reduce partial shading losses caused by difficult-to-predict sources such as clouds, dust and snow; and
3. Proposing a novel method for series arc fault detection in PV arrays.

1.4 Thesis Outline

The remainder of this thesis is structured as follows:

Chapter 2 gives a literature survey on the photovoltaic systems.

Chapter 3 gives the methodology for photovoltaic array modeling.

Chapter 4 presents the formulation for the optimal total-cross-tied interconnection for photovoltaic arrays.

Chapter 5 presents the formulation for optimal photovoltaic array reconfiguration.

Chapter 6 presents a novel series arc fault detection algorithm.

Chapter 7 makes some conclusions based on the contents of the thesis.

Chapter 2
The Photovoltaic System

2.1 Introduction

The chapter gives a literature survey of the general PhotoVoltaic (PV) system components and performance parameters.

2.2 PV System

A PV system has the following subsystems: PV array, power conditioning, system monitoring and control, PV system-utility interface, energy storage and thermal management, as shown in Figure 2-1 [1],[9]. The PV system-utility interface and the thermal subsystems (shown in dotted line) are not present in all PV systems. PV system-utility interface is not found in standalone applications and the thermal subsystem is not found in small size applications. Each of these subsystems has its own components like DC cables, junction box, DC main switch, inverter, AC cables and meters. The PV system may have some external subsystems that can be connected to the PV system like DC loads, auxiliary power sources and AC loads. Figure 2-1 shows the external subsystems outside the PV system. The components of this system will be discussed in the following subsections.

2.2.1 Array Subsystem: Array Field

PV cell is the basic unit of the array field. It is the device that transforms the sun's photons directly into electricity. There are various types of PV cells made with different technologies available today. These types have various electrical and physical characteristics depending on the technologies used to manufacture them. A series connection of a small group of cells forms the PV sub-module. A connection of a larger number of cells forms a PV module which is the smallest complete environmentally-protected assembly of PV cells and related components such as interconnects and mountings that accepts un-concentrated sunlight. Table 2-1 shows a comparison between different PV cell and module technologies in terms of efficiency [1].

A PV panel is one or more PV modules assembled, wired and designed to provide a field installable unit, while a PV array is the smallest installed assembly of PV panels or modules, support structures, foundations and other required components such as trackers [9]. PV arrays can be connected in Series Parallel (SP), Total Cross Tied (TCT), Bridge Linked (BL) or Honey Comp (HC) style in order to get the required current and voltage ratings, as shown in Figure 2-2. PV array

subfield contains one or more arrays with a distinguishing feature such as field geometry or electrical connection, while the PV field is the aggregation of all subfields. Figure 2-3 shows the different components of the array field.

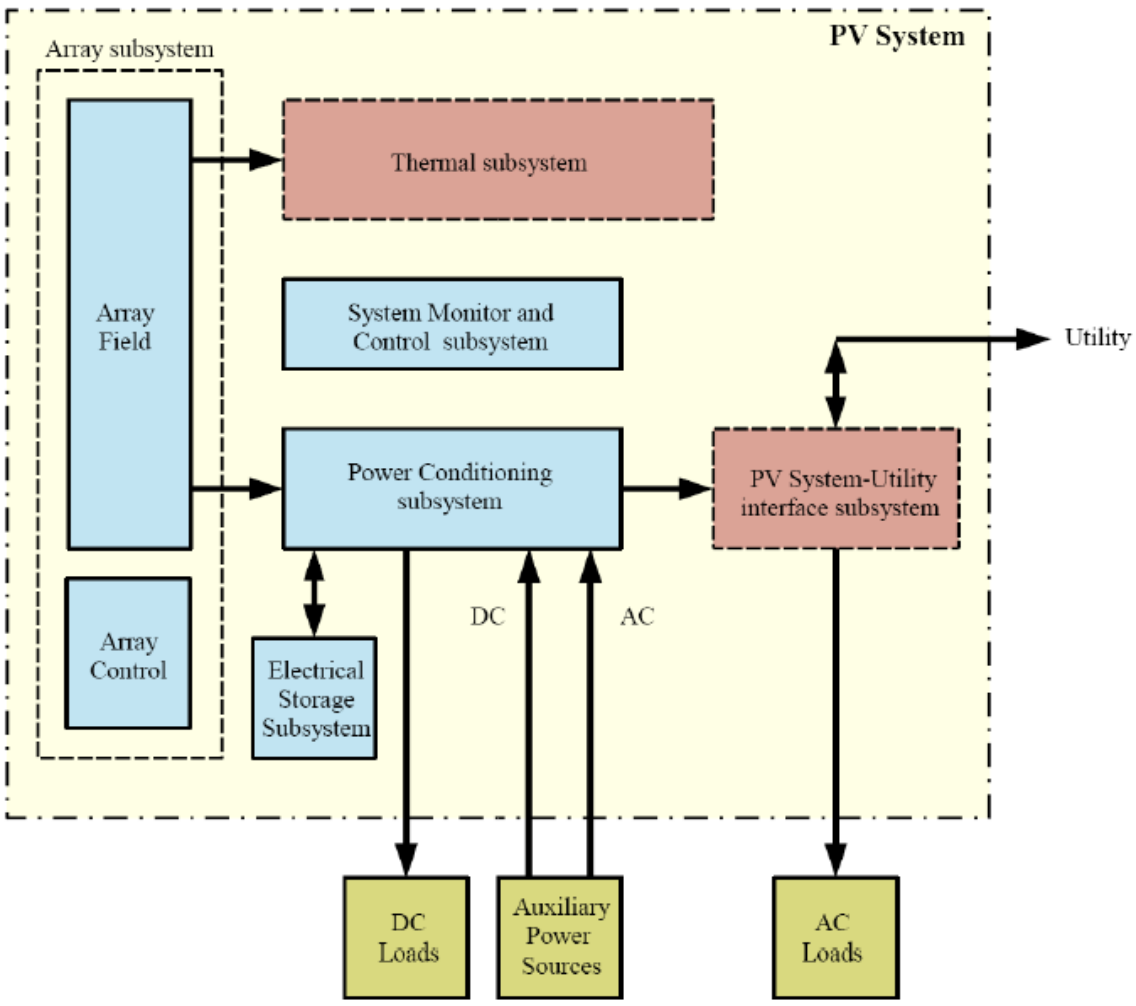

Figure 2-1: Block Diagram of general PV system

Table 2-1: Terrestrial cell and module efficiencies measured under STC*

Solar cell material	Cell efficiency (laboratory) (%)	Cell efficiency (production) (%)	Module efficiency (production) (%)
Mono-crystalline silicon	24.7	21.5	16.9
Polycrystalline silicon	20.3	16.5	14.2
Ribbon silicon	19.7	14	13.1
Crystalline thin- film silicon	19.2	9.5	7.9
Amorphous silicon	13	10.5	7.5
Micromorphous silicon	12	10.7	9.1
CIS	19.5	14	11
Cadmium telluride	16.5	10	9
III - V semiconductor	39	27.4	27
Dye-sensitized cell	12	7	5
Hybrid HIT solar cell	21	18.5	16.8

*STC stands for Standard Test Conditions.

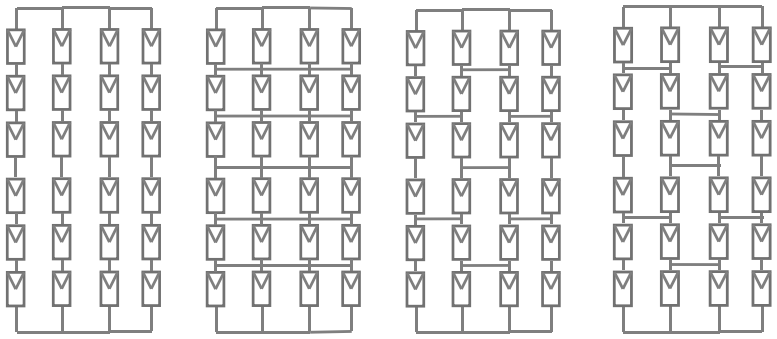

(a) (b) (c) (d)

Figure 2-2: (a) 6 x 4 SP interconnection; (b) 6 x 4 TCT interconnection; (c) 6 x 4 BL interconnection; (d) 6 x 4 HC interconnection.

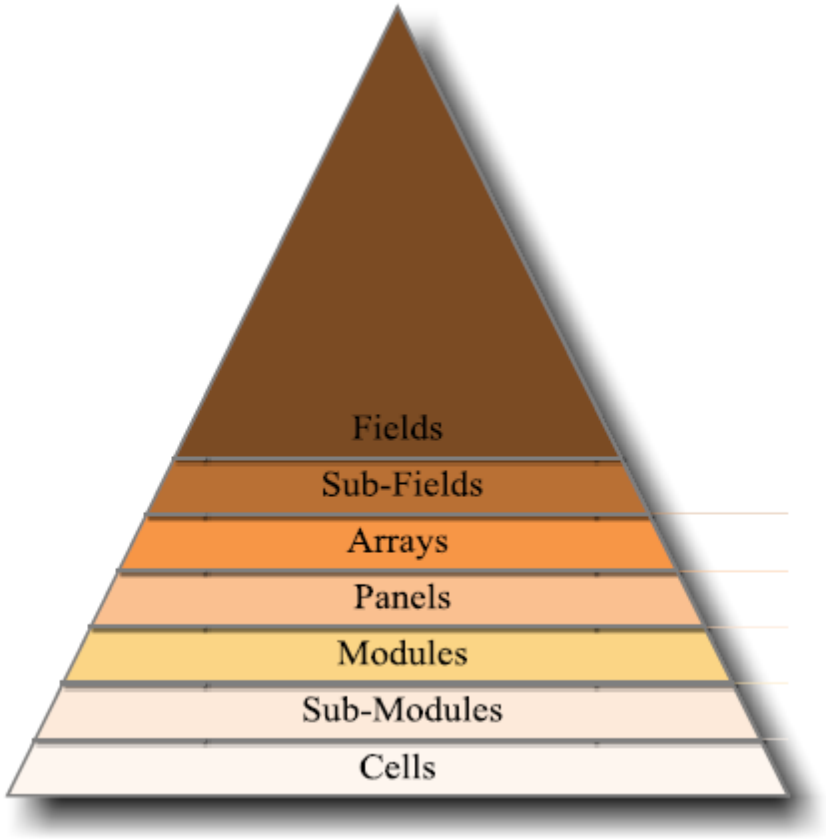

Figure 2-3: Decomposition of array field

2.2.2 Array Subsystem: Array Control

Array control means all electrical and mechanical controls that ensure proper electrical and thermal performances of the array field [1]. This can be divided into array tracking modes and array cooling methods. Array tracking modes change the tilt angle of the array in order to track the sun. There are three tracking modes which are fixed, one-axis and two-axis, as described in Table 2-2. The cooling of PV arrays is important to operate at higher efficiencies and this could be achieved by passive (air) or forced (liquid) cooling [10].

Table 2-2: Array tracking modes

Mode	Description
Fixed	Fixed tilt angle from the horizontal, but can be adjusted several times throughout the year.
One-axis	Follows the sun from east to west throughout the day in one axis.
Two-axis	Follows the sun from east to west throughout the day in two axes.

2.2.3 Power Conditioning Subsystem

This subsystem converts the dc power from the array subsystem to dc or ac power that is compatible with system requirements [1]. Its main components are Maximum Power Point Tracking (MPPT), DC-DC or/and DC-AC converter and controller. There are three main concepts for power conditioning subsystems, i.e., central, string and modular, as shown in Figure 2-4. Each of these subsystems has its own specifications and characteristics. Table 2-3 shows a comparison of these different concepts [9], [11].

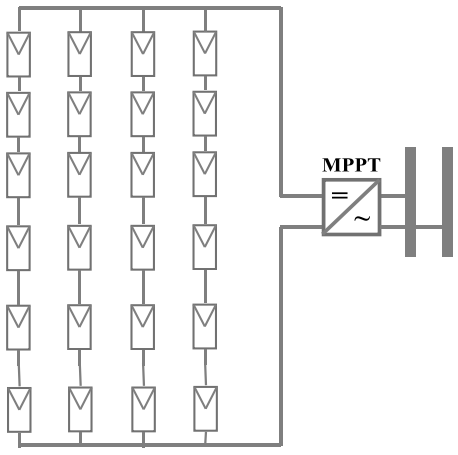

(a)

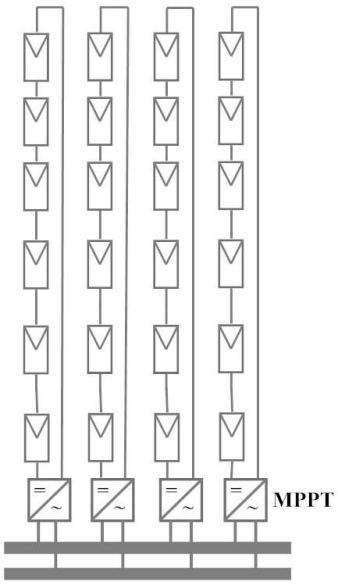

(b)

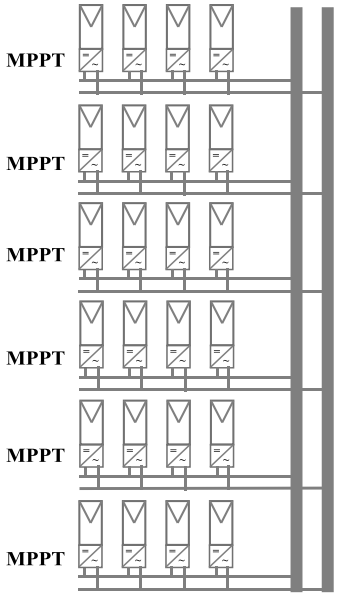

(c)

Figure 2-4: (a) Central inverter concept; (b) String inverter concept; (c) Modular inverter concept

Table 2-3: A comparison of different power conditioning concepts

	Central	String	Modular
DC voltage	High	High	Low
MPPT	Single	Multiple	Many
Partial Shading losses	Highest	High	Very little
String diodes	yes	No	No
Main DC cable	yes	No	No
DC cable junctions	yes	No	No
Inverter efficiency	Highest	Intermediate	lowest
Inverter monitoring	Easiest	Easy	Most difficult
Inverter thermal stress	Low	Low	Highest
Flexibility	Non-flexible	Flexible	Very flexible
Total cost	Higher	Lowest	Highest
Ratings	Up to several megawatts	Up to 3 kW/string	Up to 500 W/module

2.2.4 Energy Storage Subsystem

It is the sub-system that stores energy. Current technologies enable different means of energy storage [1]. Common among these are: batteries, super-capacitors, fly wheels, and super-conducting magnetic energy storage [12].

2.2.5 System Monitoring and Control Subsystem

It is a logic and control circuitry that supervises the overall operation of the system by controlling the interaction between all subsystems [1]. This system allows the detection of faults and failures of operation. There are three techniques to monitor the system: (i) Internet-based, (ii) web-based and (iii) presentation and visualization-based [9].

2.2.6 Thermal Subsystem

It is the sub-system that receives thermal energy from the array sub-system [1]. The thermal energy may be utilized for a thermal load application or dissipated. This subsystem could be found or not found in the PV system depending on the system size. The cooling is important for PV arrays in order to increase the efficiency and life time [9].

2.2.7 PV System Utility Interface Subsystem

It is the interconnection between the power conditioning subsystem, the on-site AC loads, and the utility [1]. This system may include the AC cable and the protection equipment used to connect the inverter to the grid. This system is not found in standalone applications [9].

2.2.8 External Subsystems

A PV system can serve DC or AC loads and it can be connected to other power sources such as Distributed Energy Resources (DER).

2.3 Performance Parameters of PV cells

Performance parameters of PV cells allow comparison of different types of cells. These parameters are calculated at Standard Test Conditions (STC) according to IEC standard 60904 [9]. This standard defines STC as follows:

1. Vertical irradiance of 1000 W/m^2.
2. Cell temperature of 25 ^{o}C with a tolerance of ± 2 ^{o}C.
3. Defined light spectrum according to IEC 60904-3 with an air mass of AM=1.5.

The performance parameters are as follows:

1. ***Maximum Power Point (MPP)*** which is the point on the I-V characteristic at which the solar cell works at maximum power.
2. ***MPP Voltage and current (V_{MPP}, I_{MPP})*:** the voltage and current at MPP.
3. ***Short circuit current (I_{sc})***: the current at zero output voltage.
4. ***Open circuit current (V_{oc})*:** the voltage at zero output current.
5. ***Fill Factor (FF)*** which describes the quality of the solar cell by dividing the MPP by the product of open circuit voltage and short circuit current, as in Equation (2-1). This factor is affected by the values of series and shunt resistances.

$$FF = \frac{MPP}{V_{oc} \times I_{sc}} \ \% \tag{2-1}$$

6. ***Efficiency (η)*** is the percentage of power converted from light to electricity, as in Equation (2-2), where I_r is the irradiance at STC and A_c is the surface area of the solar cell.

$$\eta = \frac{MPP}{Ir \times A_c} \times 100 \quad (2\text{-}2)$$

2.4 PV System Performance Parameters

PV systems have performance parameters developed by International Energy Agency, Photovoltaic Power Systems Program and described in the IEC standard 61724. These parameters are used to detect operational problems, compare different PV systems which differ in technology, design or geographic location, validate models for system performance estimation during the design process [13]. These parameters are:

1. ***Final PV system yield (Y_f)*** which is defined as the net energy output (E) in kWh divided by the name plate dc power P_{dc} in kW of the PV system, as shown in Equation (2-3). Its unit is kWh/kW or hours. Y_f represents the number of hours the PV system would operate at the rated power to provide the same amount of energy. Y_f normalizes the energy production with respect to the system size, thus allowing the comparison of systems of different sizes but at the same solar resource conditions.

$$Y_f = \frac{E}{P_{dc}} \quad (2\text{-}3)$$

2. ***Reference solar resource yield (Y_r)*** which is defined as the total in-plane irradiance (H) in kWh/m^2 divided by the reference irradiance (G) in kW/m^2, as in Equation (2-4). Its unit is kWh/kW or hours. Y_r represents how many hours the PV system should operate at reference irradiance G to give the same in-plane irradiance H. Y_r normalizes the solar radiation source and allows comparison of different solar sources. It is a function of the location, orientation of PV arrays and weather variability.

$$Y_r = \frac{H}{G} \quad (2\text{-}4)$$

3. ***Performance Ratio (PR)*** which is defined as the final yield (Y_f) divided by the reference yield (Y_r), as in Equation (2-5). It quantifies the overall effect of losses on the rated output power, and allows comparison of systems of different sizes under different solar resource conditions. These losses could be due to inverter inefficiency, wiring, mismatch, converting from DC to AC, module temperature, irradiance reflection, partial shading, system down time and component failure [14]. *PR* can be calculated on weekly, monthly or yearly basis. For example, if it is calculated on a weekly basis, it can indicate component failure or system

down time; if it is calculated on a monthly basis, it can indicate seasonal temperature variations; and if it is calculated on a yearly basis, it can indicate a permanent decrease in the performance. Typically, the PR is in the range of 0.6 to 0.8, but it can be less in certain periods within the year [15].

$$PR = \frac{Y_f}{Y_r} \tag{2-5}$$

2.5 Mismatch losses

Mismatch losses in PV arrays can be caused by internal sources such as manufacturing tolerance and aging, or by external sources such as partial shading. Partial shading can be caused by easy-to-predict sources such as nearby trees and arrays, and difficult-to-predicted sources such as snow, dust and clouds. Mismatch losses could be reduced by either passive or active techniques. Passive techniques use passive elements such as bypass diodes while active techniques use active elements such as solid-state switches. The most common passive technique uses bypass diodes across PV modules to reduce partial shading losses [33]. These diodes protect the modules from local heating (hot spots) and increase the overall power generation from the array under partial shading conditions. However, theses diodes do not allow the array to produce the maximum possible power under partial shading. Moreover, they increase the complexity of MPPT by creating multiple local maxima in the array's P-V characteristic [27]. Another passive technique is based on changing PV array interconnections. PV arrays can be interconnected in Series Parallel (SP), Total Cross Tied (TCT), Bridge Linked (BL) or Honey Comb (HC) style in order to get the required current and voltage ratings. In SP interconnection, modules are connected in series forming strings; then, theses strings are connected in parallel. However, in TCT interconnection, the modules are connected in parallel; then, these parallel circuits are connected in series. BL and HC could be seen as interconnections somewhere in-between the two extreme cases of SP and TCT.

TCT, BL and HC reduce mismatch losses from partial shading when compared to SP [35-37], [67-68]. However, the reduction is higher in case of TCT interconnection than that in case of BL [67] or HC [68]. In [69], the authors developed an algorithm to select the best interconnection among SP, TCT, BL and HC for certain shading situations. They found TCT to be the best interconnection for almost all partial shading situations. Partial shading affects the modules' short circuit currents, thus affecting the modules' output currents at their MPPs. This leads to lack of coherence between modules' MPPs and array's MPP. In the case of SP, this issue is more severe than that in case of

TCT. The reason is that SP has a higher number of series strings than TCT. Also, TCT interconnection reduces the possibility of turning the bypass diodes ON, thus reducing the corresponding losses. When it comes to manufacturing tolerance mismatch, TCT can indeed reduce mismatch losses when compared to SP [36]. However, these losses are now falling below 1 % due to technological advances. Theoretical studies on reliability of PV arrays show that TCT interconnection is more reliable than SP and is capable of doubling the operational lifetime of the array [38]. The reason is that TCT has more parallel circuits than SP. The manufacturing cost of TCT-connected modules has been investigated by [35]. The investigation shows that there is no reason for TCT-connected modules to have a higher cost than SP-connected modules in mass production.

Active techniques for reducing partial shading losses could be grouped into three categories: (i) Distributed Power Electronics; (ii) Multi-level inverters; and (iii) PV array reconfiguration. In distributed power electronics, each module or group of modules has its own MPPT, thus avoiding partial shading losses caused by the incoherence between the modules. Also, this technique avoids the installation of bypass diodes, thus avoiding the corresponding losses. Moreover, the MPPT detection is easier and does not require complicated algorithms. However, this technique requires additional components for each module or group of modules, such as DC-DC or DC-AC converters. Moreover, it suffers from module level partial shading and requires complicated control architectures [20-21]. Multi-level inverter topologies such as diode-clamped, capacitor clamped and cascaded H-bridge have been used to reduce partial shading losses by independent voltage control of each module. These inverters reduce the device voltage stress as well as the ac output voltage harmonics. However, they require a complicated control algorithm to achieve operation at the optimal power point and they suffer from module-level and array-level partial shading [22-23].

The reconfigurable PV array was first proposed by Salameh et al. to start and operate permanent magnet dc motor coupled to volumetric water pump [43-44]. Then, it was proposed by [45] to start and accelerate electric cars using a number of PV modules. In [46], Sherif and Boutros proposed a reconfiguration scheme for PV modules using transistors as switches between cells. In [25], Nguyen and Lehman used reconfiguration inside PV arrays and proposed two reconfiguration algorithms. However, they did not propose any mathematical formulation for the optimal reconfiguration. They also proposed dividing the PV array into fixed and adaptive parts with a switching matrix between them. They used one column only as an adaptive part in order to reduce the number of required sensors and switches, which when high can make the scheme ineffective if the shaded area is large.

Moreover, they did not mention the necessary modifications in their algorithms to deal with higher number of reconfigurable columns. They tested the system under constant resistive load without MPPT. In [26, 47-48], Velasco et al. used reconfiguration for grid connected PV arrays and proposed a mathematical formulation for it. However, the formulation was for a fully reconfigurable array only and did not indicate directly the global optimal reconfiguration. Moreover, they proposed the irradiance equalization index as the difference between the maximum and the minimum average row irradiance levels in the array. They claimed that minimization of this index could result in an optimal reconfiguration. However, optimal reconfiguration requires that all the differences between row irradiance levels are minimized, as will be shown in this chapter. They proposed a solution algorithm that required an off-line determination of all possible configurations of the PV modules. Then, the best configuration for the current shading condition was found on-line. They tested the system using six PV modules and identified 15 possible configurations. Also, they found that nine PV modules will have 280 possible configurations. The number of possible configurations will increase for larger PV arrays, making it very difficult to find the optimal configuration in a timely manner. It can be concluded that the algorithm proposed in [26, 47-48] is more suitable for small number of PV modules.

2.6 Summary

This chapter gave a brief literature survey of Photovoltaic system and its subsystems. Also, the performance parameters for photovoltaic cell and systems and mismatch losses were introduced.

Chapter 3
Modeling and Simulation for Partial Shading Study

3.1 Introduction

The purpose of this chapter is to model and simulate PV arrays in order to study the effects of partial shading on *P-V* and *I-V* characteristics, hot spots and generated power. The models can also be used to study the use of by-pass diodes and different PV interconnection styles to reduce partial shading effects. Different interconnections of PV arrays will be presented in this chapter.

In this chapter MATLAB/SIMULINK is used to model and simulate PV systems under partial-shading condition, which is a basic requirement for the next chapters. The model is user friendly for data inputting and displaying output results and it can be easily changed for different PV configurations. The following subsections will give modeling and simulation for PV cells, modules, arrays and farms.

3.2 PV Cell

The PV cell is modeled using the single diode model shown in Figure 3-1. This model is composed of a current source, a diode and two resistors. The accuracy of this model is high enough for comparison of different designs in terms of partial shading [20]. Equations (3-1) to (3-3) describe this model.

$$I_{sc} - I_D - \frac{V_D}{R_P} - I_C = 0 \tag{3-1}$$

$$I_D = I_o(e^{\frac{V_D}{V_T}} - 1) \tag{3-2}$$

$$V_C = V_D - R_S I_C \tag{3-3}$$

where I_{sc} is the PV cell short circuit current, I_D the diode current, I_o the reverse bias diode saturation current, I_C the PV cell output current, V_D the voltage across the diode, V_T the thermal voltage, V_C the PV cell output voltage, R_P the parallel resistance and R_s the series resistance. These three equations could be written in the form shown in (3-4) by substituting (3-2) and (3-3) in (3-1).

$$f(V_C, I_C) = 0 \tag{3-4}$$

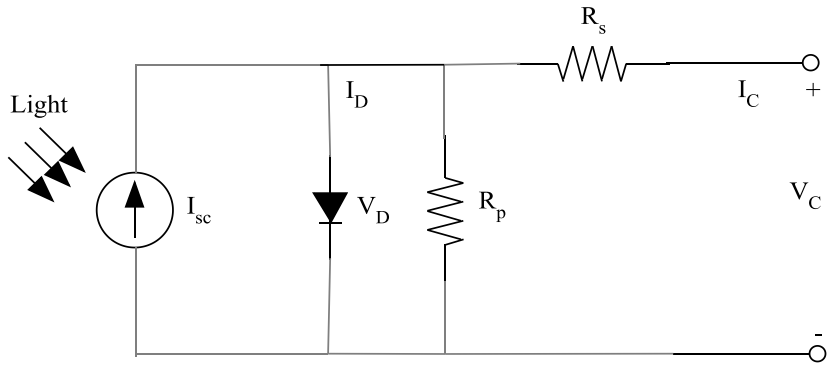

Figure 3-1: PV cell model

3.3 PV Module

PV module is modeled as a group of PV cells which could be connected in Series-Parallel (SP) or Total-Cross-Tied (TCT) style in order to get the required voltage and current. Figure 3-2 shows the SP connection for PV modules. The equations (3-5) to (3-9) describe this model.

$$I_M = \sum_{j=1}^{n} I_j \tag{3-5}$$

$$V_M = \sum_{i=1}^{m} V_C(i,j) \;\; \forall\, j \tag{3-6}$$

$$f\big(V_C(i,j), I_C(i,j)\big) = 0 \;\forall\, i,j \tag{3-7}$$

$$I_C(i,j) = I_j \;\forall\, i,j \tag{3-8}$$

$$P_M = V_M I_M \tag{3-9}$$

where V_M is the module voltage, I_M the module current, P_M the module generated power, I_j the branch current, n the number of branches , m the number of series cells, i a row index and j a column index. For the purpose of simulation, a commercial PV module, i.e., Shell Power Max Ultra SQ85-P, has been selected. The parameters of this module are given in Appendix A. Figure 3-3 and Figure 3-4 show the *I-V* and *P-V* characteristics of this module at different irradiance levels.

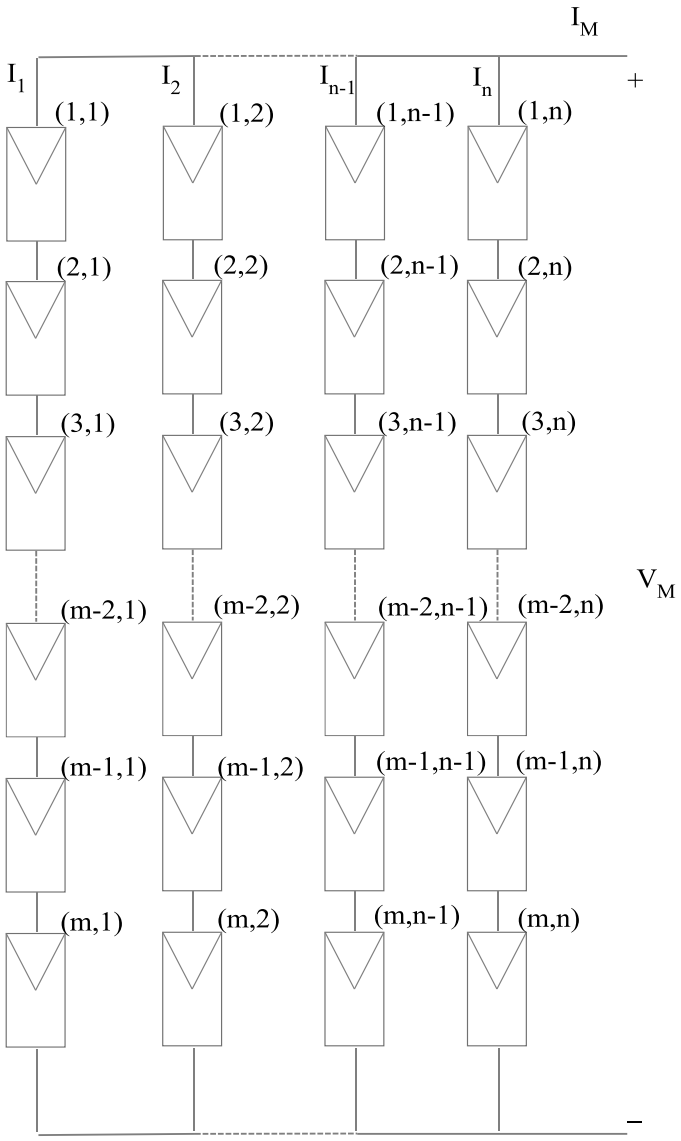

Figure 3-2: PV module connected in series-parallel style

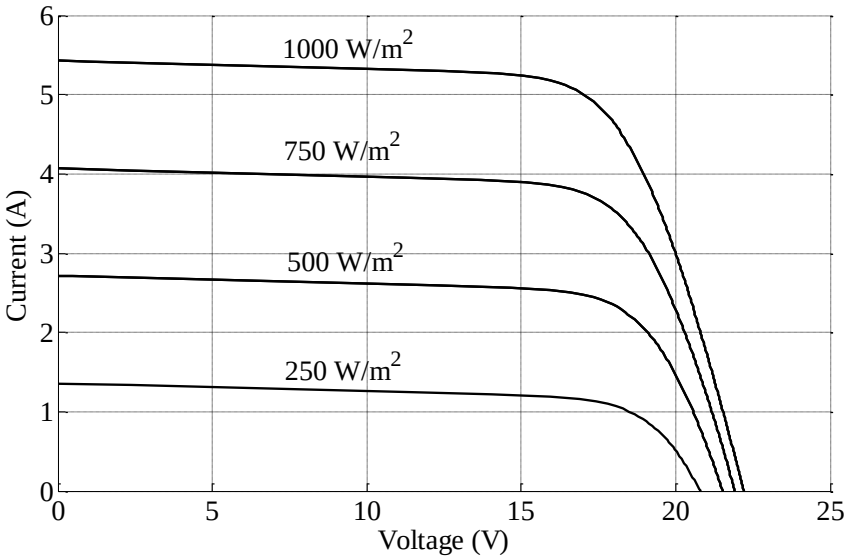

Figure 3-3: *I-V* characteristics of Shell SQ85-P module

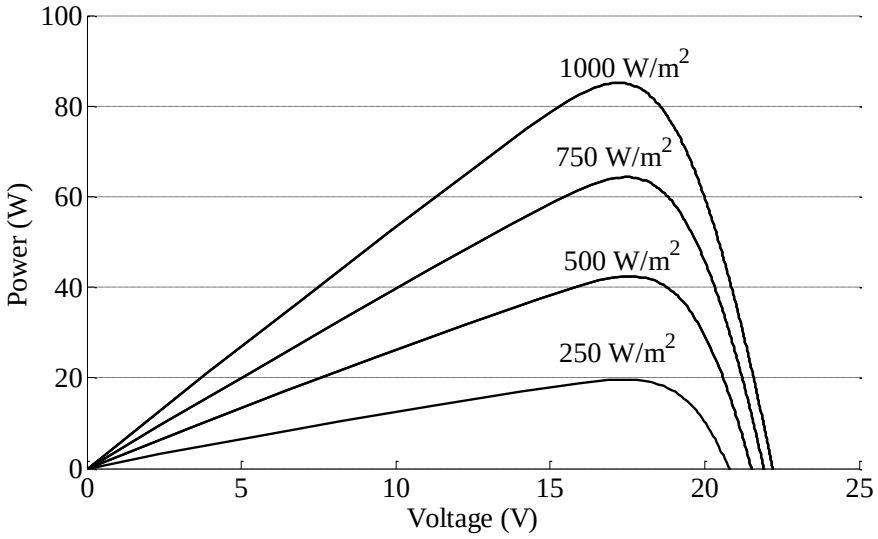

Figure 3-4: *P-V* characteristics of Shell SQ-85P module

3.4 PV Array

PV arrays can be connected in SP or TCT style, as mentioned in the previous chapter. Each of these connections styles has its own model. The SP model is like the module model shown in Figure 3-2 after replacement of cells by modules. Equations (3-10) to (3-14) describe this model:

$$I_A = \sum_{j=1}^{n} I_j \tag{3-10}$$

$$V_A = \sum_{i=1}^{m} V_M(i,j) \;\; \forall\, j \tag{3-11}$$

$$f\big(V_M(i,j), I_M(i,j)\big) = 0 \;\forall\, i,j \tag{3-12}$$

$$I_M(i,j) = I_j \;\forall\, i,j \tag{3-13}$$

$$P_A = V_A I_A \tag{3-14}$$

where V_A is the array voltage , I_A the array current, P_A the array generated power, I the branch current, n the number of branches , m the number of series modules, i a row index and j a column index. For TCT connection shown in Figure 3-5, the model is described by Equations (3-15) to (3-19).

$$I_A = \sum_{j=1}^{n} I_M(i,j) \quad \forall\, i \tag{3-15}$$

$$V_M(i,j) = V_i \;\; \forall\, i,j \tag{3-16}$$

$$V_A = \sum_{i=1}^{m} V_i \tag{3-17}$$

$$f\big(V_M(i,j), I_M(i,j)\big) = 0 \;\forall\, i,j \tag{3-18}$$

$$P_A = V_A I_A \tag{3-19}$$

A simulation for a 6 × 4 PV array under uniform irradiance level condition is performed when the array is connected in SP and TCT. The results are shown as in Figure 3-6 and Figure 3-7. The simulation results of the PV array under non-uniform irradiance levels given in Figure 3-8 are shown in Figure 3-9, where the numbers indicate irradiance levels in W/m^2. The results show that TCT connection generates more power than SP during partial shading. Figure 3-10 shows that the use of by-pass diodes across each module increases generated power as well as the number of peaks in the *P-V* characteristics.

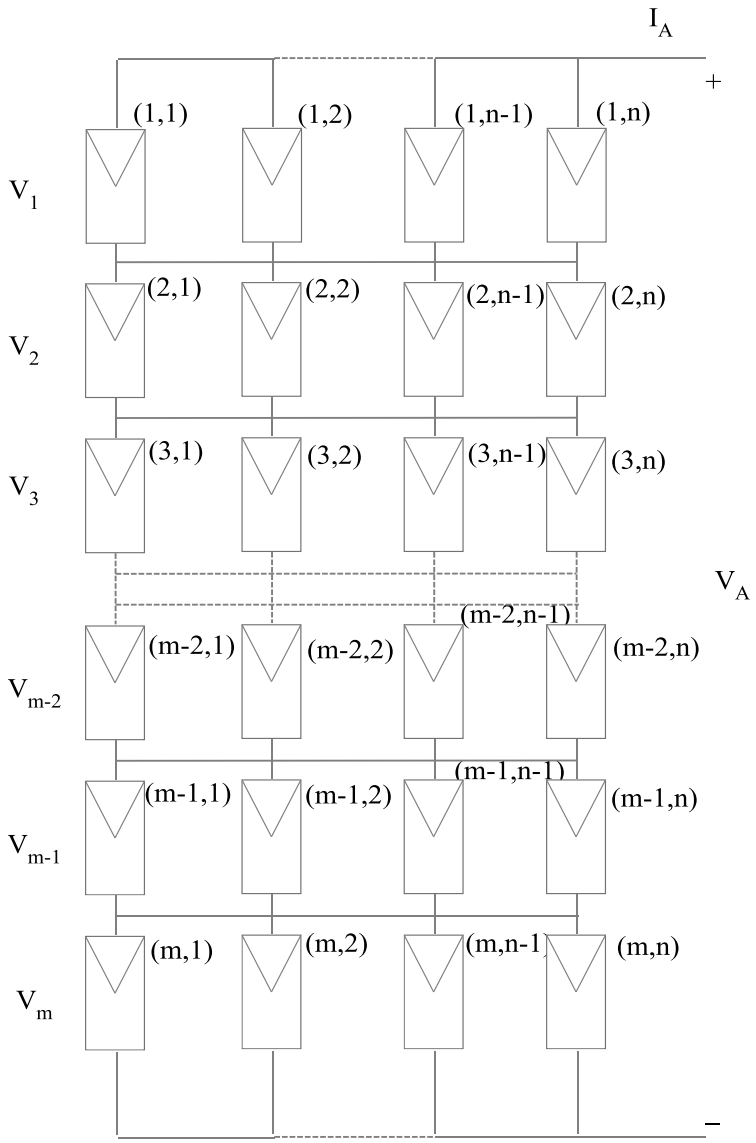

Figure 3-5: PV array connected in TCT

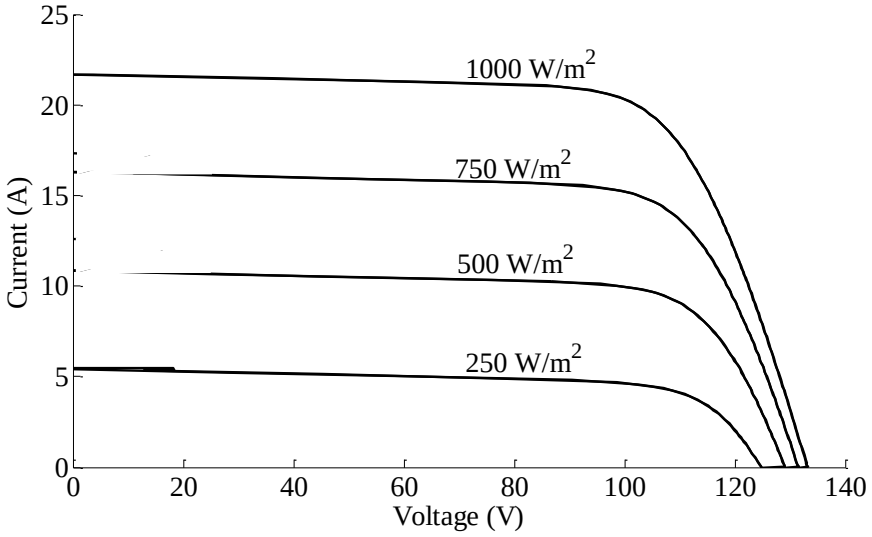

Figure 3-6: *IV* characteristics of the PV array

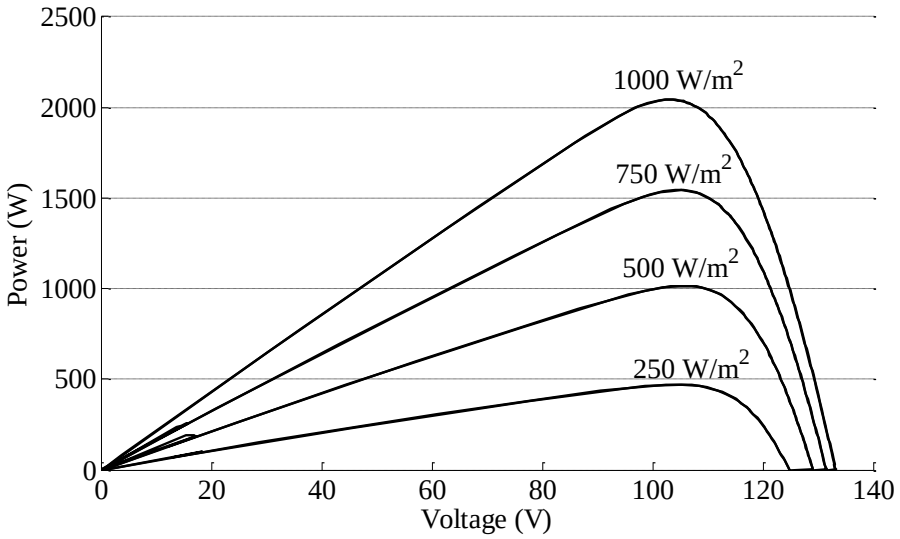

Figure 3-7: *PV* characteristics of the PV array

1000	1000	1000	1000
1000	1000	1000	1000
1000	1000	1000	1000
0	0	1000	1000
0	0	1000	1000
0	0	1000	1000

Figure 3-8: Non-uniform irradiance condition

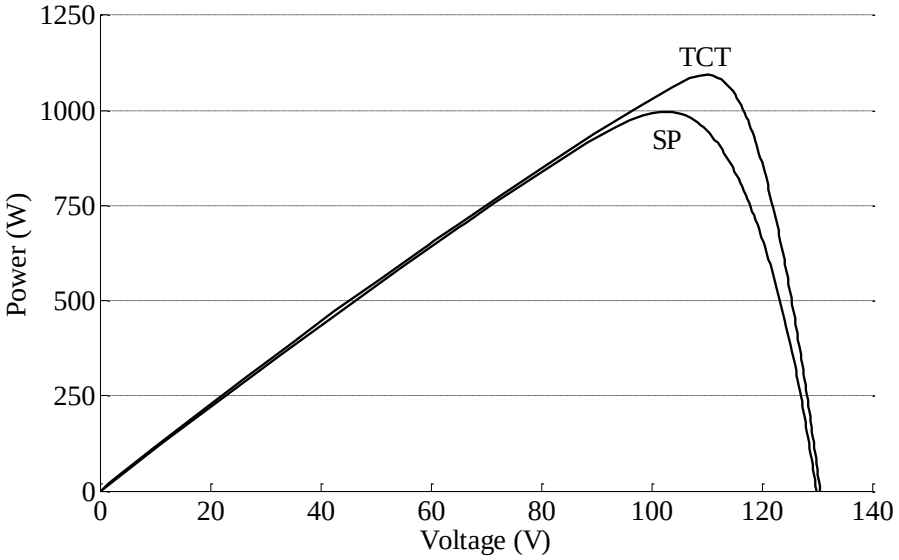

Figure 3-9: PV characteristics for non-uniform irradiance levels without by-pass diodes

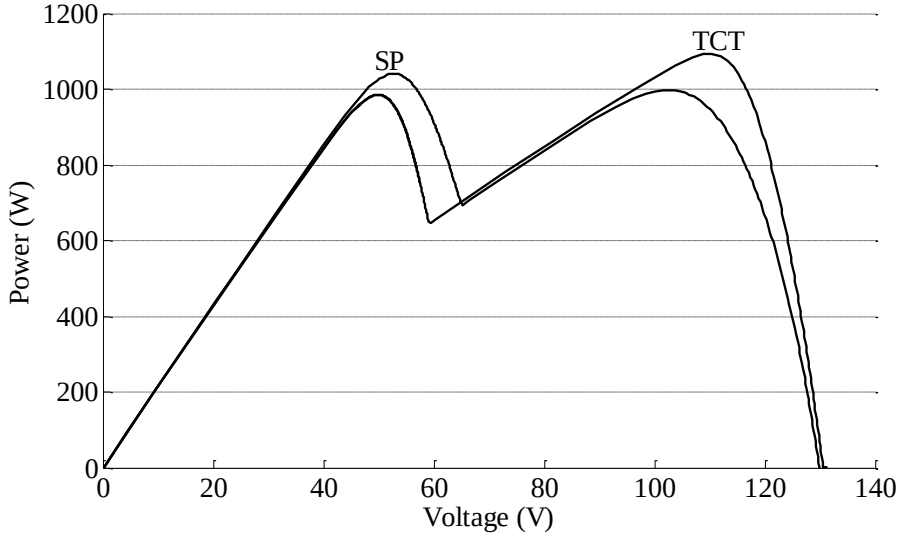

Figure 3-10: PV characteristics for non-uniform irradiance levels with by-pass diodes

3.5 PV Farm

PV farm has three concepts as mentioned in chapter 2; these are central, string and modular. The model for the central concept is similar to that of the SP PV array shown in Figure 3-2 and is given by Equations (3-20) to (3-24). The model for the modular concept is exactly the same as the array model.

$$I_F = \sum_{j=1}^{n} I_j \tag{3-20}$$

$$V_F = \sum_{i=1}^{m} V_A(i,j) \ \forall \ j \tag{3-21}$$

$$f\big(V_A(i,j), I_A(i,j)\big) = 0 \ \forall \ i,j \tag{3-22}$$

$$I_A(i,j) = I_j \ \forall \ i,j \tag{3-23}$$

$$P_F = V_F I_F \tag{3-24}$$

where V_F is the farm voltage , I_F the farm current, P_F the farm generated power, I the branch current, n the number of branches , m the number of series arrays, i a row index and j a column index. The model for string concept shown in Figure 3-11 is given by Equations (3-25) to (3-28).

$$I_F = I_A(i) \ \forall \ i \tag{3-25}$$

$$V_F = \sum_{i=1}^{m} V_A(i) \tag{3-26}$$

$$f\big(V_A(i), I_A(i)\big) = 0 \ \forall \ i \tag{3-27}$$

$$P_F = V_F I_F \tag{3-28}$$

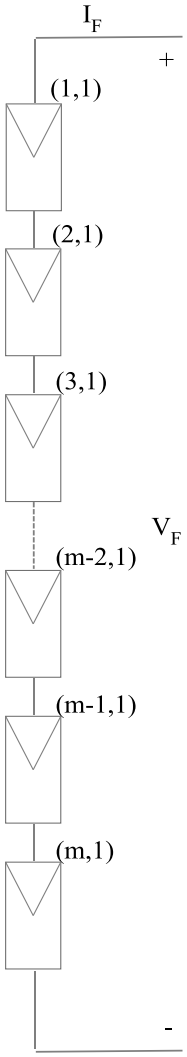

Figure 3-11: String PV farm concept

3.6 Summary

This chapter presented the mathematical models and simulation results for PV cells, modules, arrays and farms. The models are nonlinear and their nonlinearity increases with the system size. A simplified cell model which is suitable for partial shading study is selected to reduce computational efforts. The solution of these models is done using MATLAB/SIMULINK in a user-friendly environment for data inputting and for getting output results. The simulated model can be changed easily to be used with any design or configuration.

Chapter 4
Optimal Total-Cross-Tied Interconnection to Reduce Mismatch Losses

4.1 Introduction

PV farm installations require tens of acres of land to avoid partial shading caused by consecutive rows of PV arrays. The arrays are usually installed in landscape instead of portrait to avoid partial shading caused by consecutive rows, thus increasing installation cost. In addition to PV farms, Building Integrated Photovoltaic (BIPV) installations usually suffer from partial shading caused by nearby objects such as trees and buildings.

This chapter proposes new interconnection schemes for PV arrays that can significantly reduce partial shading losses caused by easy-to-predict sources such as consecutive rows, buildings and trees. The chapter is organized as follows. First, mismatch losses and PV array interconnection schemes are presented. Then, the proposed optimal total-cross-tied interconnection scheme is introduced. The optimal cross-linked interconnection is presented next, followed by the solution methodology and simulation model. Finally, some application case studies are presented.

4.2 Mismatch Losses

PV arrays are normally composed of large numbers of PV modules. These PV modules can have different current-voltage (I-V) characteristics. The difference between module characteristics is called I-V mismatch. I-V mismatch can have permanent or temporary sources.

Permanent sources cause I-V mismatch by changing one or more parameter in the PV module such as the value of parallel resistance and/or series resistance. Permanent sources include manufacturing tolerance, performance degradation and module cracking. Power loss from manufacturing tolerance mismatch is below 1% for modern Si-modules [16]. These mismatch losses could increase to up to 2.4% due to aging [17].

A temporary source for I-V mismatch is changes in the irradiance level received by PV modules. I-V mismatch caused by the changes in irradiance level is called partial shading of PV array. Furthermore, partial shading sources could be divided into easy-to-predict and difficult-to-predict sources. Easy-to-predict sources include nearby PV arrays, buildings and trees. Examples for difficult-to-predict sources are clouds, soiling and snow. Partial shading loss reduces annual energy yield by 5-10 % in

Building Integrated Photovoltaic (BIPV) systems [18-19] and by 3- 6% in PV farms [20]. I-V mismatch causes power losses in PV arrays via the following four mechanisms:

4.2.1 Array Maximum Power Point (MPP) is not coherent with those of the individual modules

Each module in the PV array should operate at its own maximum power point in order to maximize the power production of the PV array. This can be ensured by a single Maximum Power Point Tracker (MPPT) if there is no mismatch between the modules. In case of mismatch, there is no guarantee that all the modules are operating at their Maximum Power Points (MPPs). This can be avoided by having a dedicated MPPT for each PV module [21-22]. Another solution is to use a multilevel inverter with independent voltage control for each PV module [23-24]. In [25], it is proposed to connect all the modules in parallel to avoid these losses. The proposed solutions in [21-25] require additional components and circuits that can increase the system complexity and cost. In [26-27], it is proposed to use switches and sensors to reconfigure the PV array to achieve higher coherence among the modules' MPPs. The proposed approach in [26-27] is dynamic and requires sensors and switches; however the approach proposed in this chapter is static and does not require any sensors or switches.

4.2.2 MPPT is misled by existence of multiple MPPs

Some PV arrays are supplied with bypass diodes across their modules. Under I-V mismatch, these diodes create multiple MPPs for the PV array. These MPPs can mislead the MPPT and make it identify a local optimal point as the global maximum point, leading to reduction in generated power [28]. This problem has been investigated by many researchers who have developed better MPPT algorithms that can find the global maximum power point [29-32]. However, these algorithms are complex and may require high online computational effort.

4.2.3 Bypass diodes are turned ON

PV modules with bypass diodes across them will not produce any useful power when theses diodes are turned ON, although they might be capable of producing some useful power. Moreover, bypass diodes create additional power loss due to their ON resistances [33]. In [34], a new circuit is proposed to avoid bypass diode ON resistance losses. However, this circuit does not recover the power that is lost due to bypassing of the modules.

4.2.4 Reverse currents

Some parallel connected PV modules can suffer from reverse currents due to I-V mismatch. This reverse current causes these modules to absorb power instead of producing power, which reduces the production and increases the heating losses. Some PV arrays are equipped with reverse current blocking diodes to prevent reverse currents [16].

The previous discussions showed that I-V mismatch losses reduce the annual energy yield from the PV array to a great extent. The objective of the work presented in this chapter is to limit the reduction in annual energy yield.

4.3 Interconnection Schemes

PV modules can be interconnected in four main styles: (i) Series Parallel (SP), (ii) Total Cross Tied (TCT), (iii) Bridge linked (BL) and (iv) Honey Comb (HC) , as shown in Figure 4-1.

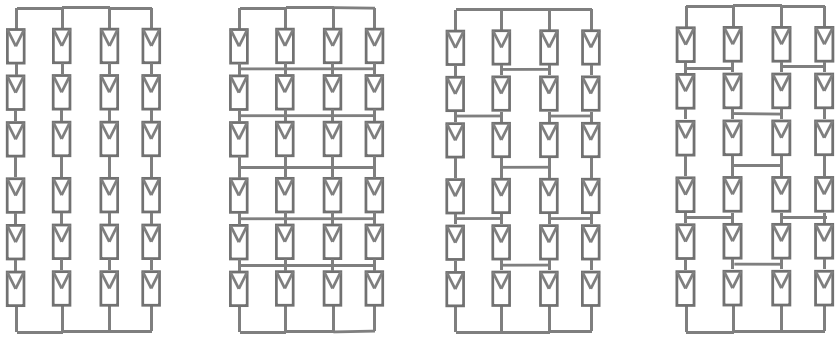

(a) (b) (c) (d)

Figure 4-1: Main PV module interconnection styles: (a) 6 × 4 SP interconnection, (b) 6 × 4 TCT interconnection, (c) 6 × 4 BL interconnection and (d) 6 × 4 HC interconnection.

In SP interconnection, modules are connected in series forming strings; then, theses strings are connected in parallel. However, in TCT interconnection, the modules are connected in parallel; then, these parallel circuits are connected in series. BL and HC could be seen as interconnections somewhere in-between the two extreme cases of SP and TCT.

TCT, BL and HC reduce mismatch losses from partial shading when compared to SP [35-37], [67-68]. However, the reduction is higher in case of TCT interconnection than that in case of BL [67] or HC [68]. In [69], the authors developed an algorithm to select the best interconnection among SP, TCT, BL and HC for certain shading situations. They found TCT to be the best interconnection for

almost all partial shading situations. Partial shading affects the modules' short circuit currents, thus affecting the modules' output currents at their MPPs. This leads to lack of coherence between modules' MPPs and array's MPP. In the case of SP, this issue is more severe than that in case of TCT. The reason is that SP has more number of series strings than TCT. Also, TCT interconnection reduces the possibility of turning the bypass diodes ON, thus reducing the corresponding losses.

When it comes to manufacturing tolerance mismatch, TCT can indeed reduce mismatch losses when compared to SP [36]. However, these losses are now falling below 1 % due to technological advances.

Theoretical studies on reliability of PV arrays show that TCT interconnection is more reliable than SP and is capable of doubling the operational life time of the array [38]. The reason is that TCT has more parallel circuits than SP. The manufacturing cost of TCT-connected modules has been investigated by [35]. The investigation shows that there is no reason for TCT-connected modules to have a higher cost than SP-connected modules in mass production.

The previous discussion shows the superiority of TCT connection over SP in terms of lower mismatch losses and higher reliability. Also, it shows that the manufacturing cost of TCT could be similar to that of SP. Therefore, TCT connection will be used as a starting point to build upon in this work.

4.4 Optimal-Total-Cross-Tied Interconnection

In practice, partial shading analysis is performed in the planning stage, i,.e., before building the PV field [9], to predict the possible partial shading situations. The results indicate the shading pattern, irradiance levels and duration (t_g) for each partial shading situation and the total number of partial shading situations (N). Accordingly, the OTCT interconnection scheme is derived during the planning stage. Figure 4-2 shows a number of different partial shading situations.

1000	1000	1000	1000
1000	1000	1000	1000
1000	1000	1000	1000
1000	1000	1000	1000
1000	1000	1000	1000
500	500	500	500

1000	1000	1000	1000
1000	1000	1000	1000
1000	1000	1000	1000
250	250	1000	1000
250	250	1000	1000
250	250	1000	1000

1000	1000	1000	1000
1000	1000	1000	1000
1000	1000	1000	1000
1000	1000	1000	1000
500	500	500	500
500	500	500	500

1000	1000	1000	1000
1000	1000	1000	1000
1000	1000	1000	1000
0	1000	1000	1000
0	0	1000	1000
0	0	0	1000

500	500	500	500
750	750	750	500
1000	750	750	500
1000	1000	750	500
1000	1000	1000	750
1000	1000	1000	1000

Figure 4-2: A number of different Partial Shading Situations

Mismatch power losses could be caused by permanent sources or temporary sources, as discussed earlier. Temporary sources have a time component which should be taken into consideration. Therefore, this work proposes to find one TCT interconnection that maximizes array's power production under mismatch for several time segments, which results in maximum energy production under mismatch, as in (4-1). The TCT interconnection found is the Optimal-Total-Cross-Tied (OTCT) interconnection for maximizing array's generated energy under mismatch. OTCT connects the modules from the same row into different parallel circuits in such a way that energy production under mismatch is maximized. Energy production is maximized due to the increased coherence between modules' MPPs and array's MPP and due to lower probability of turning ON the bypass diodes. This is completely different than traditional TCT interconnection in which the modules from the same row are connected in one parallel circuit without any maximization of generated energy.

$$\text{Maximize } \mathrm{EA} = \sum_{g=1}^{N} \mathrm{VA_g IA_g t_g} \quad (4-1)$$

In (4-1) , $\mathrm{VA_g IA_g}$ is the array's output power at time segment g during mismatch. This power is multiplied by segment duration tg to find array's output energy during time segment g during mismatch. The total number of time segments is N The sum of all energies during different time segments will then give the array's total energy during mismatch. This formulation takes into consideration the impact of permanent and temporary sources of mismatch.

4.4.1 Existence Variable

Consider the m parallel circuits shown in Figure 4-2, where each circuit has n parallel modules. The index for parallel circuits is i and the index for modules is q. All positions in one parallel circuit are identical; therefore, there is no need for an index for the positions of modules inside the parallel circuit. However, an index j is defined for the positions of the module in the parallel circuits. This index is required to find Kirchhoff's Laws' constraints as will be shown later. An existence variable is required to find the position of module q in the OTCT interconnection to maximize the generated energy during mismatch. The existence variable can be defined as follows:

Definition: The Existence Variable y_{ijq} is defined as a binary variable such that:

$$y_{ijq} = \begin{cases} 1, & \text{if module q exists at position ij} \\ 0, & \text{otherwise} \end{cases}$$

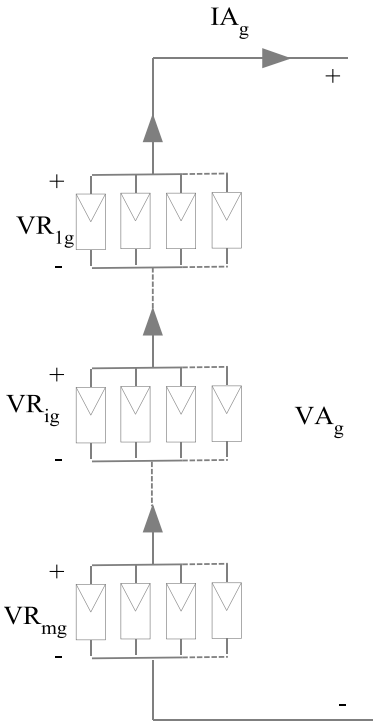

Figure 4-3: A PV array composed of m parallel circuits with n modules per parallel circuit

4.4.2 Kirchhoff's Laws' Constraints

These constraints are Kirchhoff's Current Law (KCL) and Kirchhoff's Voltage Law (KVL) for OTCT interconnection. Applying KCL to each parallel circuit means that the sum of the currents of modules in each parallel circuit is equal to the array's current. This can be mathematically formulated as

$$IA_g = \sum_{j=1}^{n} \sum_{q=1}^{m \times n} IM_{qg} y_{ijq} \qquad \forall i, g \qquad (4-2)$$

In (4-2), the current of module q at time segment g, i.e., IM_{qg}, is multiplied by the existence variable y_{ijq}. The result of this multiplication will give the module's current only if the module exists at position ij. Therefore, the summation over q will give the existing module current at position ij. It should be noted that this existing module current will be only from one module because each position will have only one module, as will be shown later by the logical constraints. After finding the existing module current, the summation over j will give the total current of the existing modules. Equation (4-

2) is repeated for each parallel circuit i for each time segment g, implying that there are m×N equations.

Applying KVL to each parallel circuit means that the voltages of all existing modules in one parallel circuit are equal to one another and equal to the row voltage VR_{ig}, as described by (4-3).

$$VR_{ig} = \sum_{q=1}^{m \times n} VM_{qg} y_{ijq} \qquad \forall i, j, g \qquad (4-3)$$

Similar to existing module current modeling, the existing module voltage is modeled by the summation over q for the multiplication of module's voltage and the existence variable. This multiplication will give the module's voltage only if module q exists at position ij. In the logical constraints section, each position will be constrained to have one module only. Therefore, the summation over q will give the voltage of the only one module that exists at position ij. This equation is repeated for each position and for each time segment, which means that there are m×n×N equations.

Applying KVL to the arrays' input means that the sum of the individual row voltages is equal to arrays' voltage, as described by (4-4).

$$\mathrm{VA_g} = \sum_{\mathrm{i=1}}^{\mathrm{m}} \mathrm{VR_{ig}} \qquad \forall \mathrm{g} \qquad (4-4)$$

In Equation (4-4), the summation over i for VR_{ig} will give the total array voltage. This equation is repeated for each time segment (i.e., N times).

4.4.3 Modules' Model Constraints

These constraints are the model equations for the PV modules. The most commonly-used models are the single-diode model and the double-diode model. Single-diode model, described by (4-5), is used in this work to reduce computational effort.

$$\mathrm{IRR_{qg}} \frac{\mathrm{I_{scq}}}{\mathrm{G}} - \mathrm{I_{0q}} \left(e^{\frac{\frac{\mathrm{VM_{qg}}}{\mathrm{N_{sq}}} + \mathrm{R_{sq}} \mathrm{IM_{qg}}}{\mathrm{V_{Tq}}}} - 1 \right) - \frac{\frac{\mathrm{VM_{qg}}}{\mathrm{N_{sq}}} + \mathrm{R_{sq}} \mathrm{IM_{qg}}}{\mathrm{R_{Pq}}} - \mathrm{IM_{qg}} = 0 \qquad \forall \mathrm{q, g} \quad (4-5)$$

Equation (4-5) is essential in development of the OTCT interconnection because it represents all sources of mismatch. Permanent sources are reflected in Iscq, Ioq, Nsq, Rsq, VTq and RPq, while

temporary sources are represented by IRRqg. This equation is repeated for each module and for each time segment (i.e., m×n×N times).

4.4.4 Logical Constraints

The logical constraints are those which must be satisfied in order to have a practical solution for the problem. The first constraint states that each position ij will have only one module q, as described by (4-6).

$$\sum_{q=1}^{m\times n} y_{ijq} = 1 \qquad \forall i,j \qquad (4-6)$$

This constraint is repeated m×n times. The second constraint states that all modules should exist (i.e., all modules must be connected), as described by (4-7).

$$\sum_{i=1}^{m}\sum_{j=1}^{n} y_{ijq} = 1 \qquad \forall q \qquad (4-7)$$

This constraint ensures that each module q will have a position ij. This constraint is repeated m×n times. It should be noted that both constraints (4-6) and (4-7) are needed. For example, if (4-6) is used alone, then the same module may exist at different positions. Also, if only (4-7) is used, then some positions will have more than one module.

4.5 Solution Algorithm and Simulation Model

The OTCT problem is a Mixed Integer Non-Linear Programming (MINLP) problem. MINLP problems can be solved by Branch and Bound (BB) algorithm. BB uses relaxation and separation to solve the MINLP problem. The strategy of BB algorithm is to solve the original MINLP problem after relaxing the integer variables, that is, to solve the Non Linear Programming (NLP) problem using an NLP solution method such as Interior Point Method (IPM). If the solution of the NLP is integer, then the global optimum is found. If not, then the NLP problem is separated into two sub-problems using an integer variable with a non-integer value. One of the sub-problems is solved and if the sub-problem is not fathomed, it should be divided into two new sub-problems. The BB process stops when all the sub-problems have been fathomed. The stored incumbent at the end of the process gives the global optimal solution [39]. The OTCT problem is a planning problem; therefore, it is

required to reach the optimal solution in a reasonable time. BB can reach the solution in a reasonable time for small- to medium-size arrays. However, for larger arrays another algorithm should be used.

A simulation model is needed to compare different interconnections (i.e., SP, TCT and OTCT). The simulation model is built in MATLAB/SIMULINK environment. This model is based on the single-diode model for PV modules, described by (4-5) and shown in Fig. 4-3 [75]. The PV array is constructed from the interconnection of PV modules in SP, TCT or OTCT interconnection style. A Bypass diode is connected across each PV module and no reverse current blocking diodes are used. It should be noted that the wiring resistance is ignored in the simulation model. The PV module data is given in Appendix A.

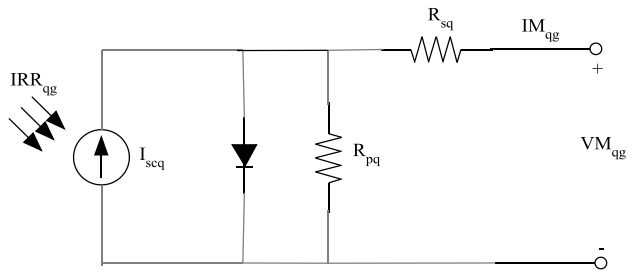

Figure 4-4 PV module single-diode model.

4.6 Performance Ratio

The array's overall Performance Ratio (PR) normalizes the effect of mismatch losses based on the rated output dc power P_{dc}, and allows comparison between arrays of different sizes under different irradiance conditions HA [13]. The PR is directly related to the overall system efficiency; a higher PR means higher system efficiency.

$$\mathrm{PR} = \frac{\mathrm{EA_{max}}}{\mathrm{HA}} \times \frac{\mathrm{G}}{\mathrm{P_{dc}}} \qquad (4-8)$$

EA_{max} and HA used in (4-8) can be found from (4-9) and (4-10), respectively.

$$\mathrm{EA_{max}} = \sum_{g=1}^{N} \mathrm{MPPA_g t_g} \qquad (4-9)$$

$$\mathrm{HA} = \sum_{g=1}^{N} \mathrm{IRRA_g t_g} \qquad (4-10)$$

The array's PR for each time segment g can then be found as follows:

$$\mathrm{PR_g} = \frac{\mathrm{MPPA_g t_g}}{\mathrm{IRRA_g t_g}} \times \frac{\mathrm{G}}{\mathrm{P_{dc}}} = \frac{\mathrm{MPPA_g}}{\mathrm{IRRA_g}} \times \frac{\mathrm{G}}{\mathrm{P_{dc}}} \quad (4-11)$$

4.7 Application Examples

In the following application examples, the focus, in particular, is on partial shading in PV fields. The three shading patterns shown in Figure 4-4 are approximations for the most common partial shading patterns in PV fields [40-42]. These patterns happen when the front-row arrays are shading the bottom of the back-row arrays, causing the overall array to be partially shaded. The irradiance levels of the shaded modules depend on the distance between the rows and the environmental conditions [40-42]. Therefore, two application examples are considered: (i) the irradiance levels of the shaded modules are 50 % of those of the un-shaded modules; (ii) the irradiance levels of the shaded modules are 25% of those of the un-shaded modules. It should be noted that each application example represents a different PV field; therefore, one OTCT interconnection is found for each field. Each situation has a time segment g such that t_g represents the total time duration of each partial shading situation throughout the year. This total time duration is assumed to be the same for all partial shading situations in these applications for simplicity and without loss of generality.

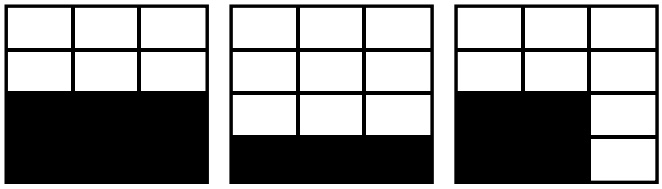

(a) (b) (c)

Figure 4-5: Three easy-to-predict partial shading situations

4.7.1 Application Example 1

In this application example, it is assumed that the irradiation level for the shaded modules is 50% of that for of the un-shaded ones, as shown in Figure 4-5, where the numbers indicates irradiance levels in W/m^2. The static OTCT interconnections for these situations can be found using the optimization model discussed earlier, as shown in Figure 4-6 (b). Figure 4-6 (a) shows the TCT interconnection for the same array, where the numbers indicate the coordinates of modules' physical positions. The

simulation model is used to compare the performance of the OTCT with those of SP and TCT interconnections for each partial shading situation.

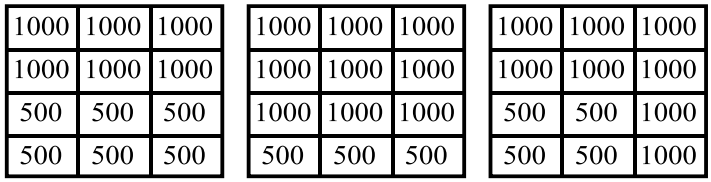

Figure 4-6: Three partial shading situations

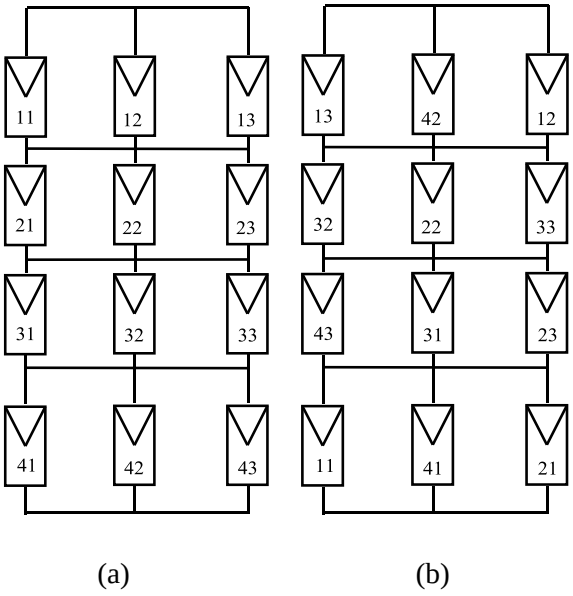

Figure 4-7: (a) TCT interconnection; (b) OTCT interconnection

4.7.1.1 Situation (a)

The comparison results for this situation are given in Table 4-1. SP and TCT interconnections suffer from partial shading losses caused by lack of coherence between the modules` MPPs and the array's MPP. The array's MPP (552 W) occurs when the modules are not at their MPPs. The MPP for the 1000 W/m^2 modules is 85 W and the MPP for the 500 W/m^2 modules is 42.2 W. However, for OTCT interconnection, the array's MPP (718 W) has more coherence with the modules' MPPs. This coherence is reflected in the array's performance ratio for this partial shading situation, which has increased from 0.72 for SP and TCT to 0.94 for OTCT. The higher coherence is also reflected in the output power which has increased by 30 % with respect to those of SP and TCT. Figure 4-6 shows

that the Power - Voltage (P-V) characteristic of OTCT interconnection is smoother than those of SP and TCT interconnections, which reduces the probability of the MPPT getting misled.

Table 4-1 Situation (a) simulation results

	Modules' powers at $MPPA_a$ (W)			$MPPA_a$ (W)	PR_a	Power change w.r.t. SP (%)
SP &TCT	51	51	51	552	0.72	---
	51	51	51			
	41	41	41			
	41	41	41			
OTCT	76	76	76	718	0.94	+30
	76	84	84			
	41	41	41			
	41	41	41			

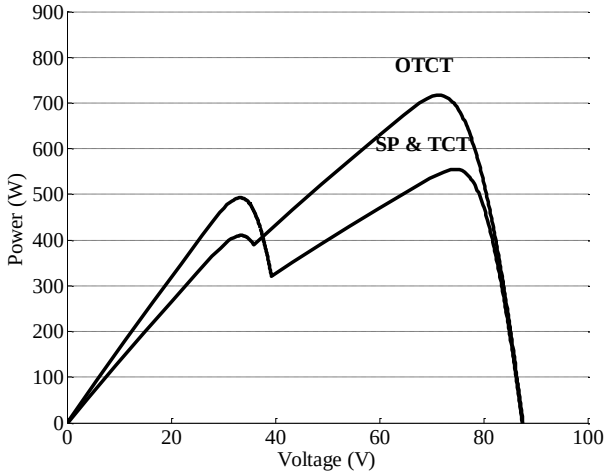

Figure 4-8 : situation (a) interconnections' P-V characteristics

4.7.1.2 Situation (b)

In this situation, SP and TCT suffer from partial shading losses caused by turning ON of some bypass diodes. These diodes bypass the 500 W/m^2 modules, thus eliminating any power produced by them. Moreover, the ON resistance for these diodes has a power loss of 3.1 W, as shown in Table 4-2. In the case of OTCT, bypass diodes are OFF; therefore, the 500 W/m^2 modules are still producing power. The impact of OTCT interconnection is increasing the performance ratio from 0.85 to 0.975, improving the generated power by 15.1 % and smoothing the P-V characteristic, as shown in Figure 4-8.

Table 4-2**:** Situation (b) simulation results

	Modules' powers at $MPPA_b$ (W)			$MPPA_b$ (W)	PR_b	Power change w.r.t. SP (%)
SP & TCT	85	85	85	755.7	0.85	---
	85	85	85			
	85	85	85			
	-3.1	-3.1	-3.1			
OTCT	85	85	85	870	0.975	+15.1
	85	78	85			
	85	78	78			
	42	42	42			

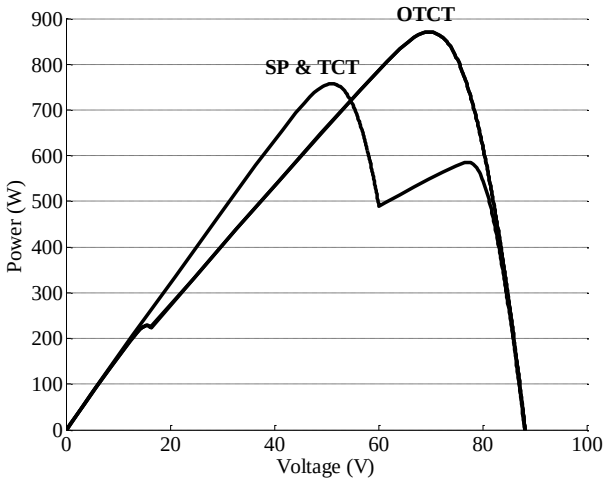

Figure 4-9 : Situation (b) interconnections' P-V characteristics

4.7.1.3 Situation (c)

In this situation, TCT has lower partial shading losses than SP because it has more coherence between modules' MPPs and array's MPP. TCT can have better coherence than SP only when the rows are partially shaded; otherwise, there is no significant difference. However, OTCT interconnection can have better coherence than SP and TCT in case of rows partial shading or full shading, as shown in the previous situations and Table 4-3. In this situation, the OTCT interconnection is able to reduce partial shading losses to zero, thus gaining a unity performance ratio. Moreover, its P-V characteristic has one peak only, as shown in Figure 4-9, thus simplifying the job of MPPT.

From the previous situations and using (4-9), the OTCT interconnection increases the annual energy yield during partial shading by 21%, when compared to SP, and by 19%, when compared to TCT.

Moreover, using (4-8), (4-9) and (4-10), the PR during partial shading for OTCT increases to 0.97 from 0.8 for SP and 0.81 for TCT.

Table 4-3 **:** Situation (c) simulation results

	Modules' powers at $MPPA_c$ (W)			$MPPA_c$ (W)	PR_c	Power change w.r.t. SP (%)
SP	52	52	84.3	700	0.824	---
	52	52	84.3			
	38.7	38.7	84.3			
	38.7	38.7	84.3			
TCT	66.3	66.3	66.3	731	0.86	+4.4
	66.3	66.3	66.3			
	41.3	41.3	84			
	41.3	41.3	84			
OTCT	85	85	85	848.8	1.00	+21.3
	85	85	85			
	42.2	42.2	85			
	42.2	42.2	85			

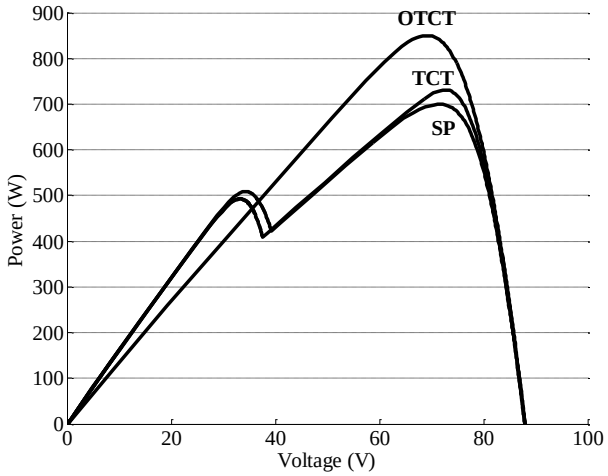

Figure 4-10: Situation (c) interconnections' P-V characteristics

4.7.2 Application Example 2

In this application example, the irradiance level of the shaded modules is 25% of that of the un-shaded ones, as shown in Figure 4-10. The static OTCT interconnection is found using the optimization model. The solution of the model gives the interconnection shown in Figure 4-11 (b) which is a modified version of the TCT interconnection of Figure 4-11 (a).

1000	1000	1000
1000	1000	1000
250	250	250
250	250	250

(a)

1000	1000	1000
1000	1000	1000
1000	1000	1000
250	250	250

(b)

1000	1000	1000
1000	1000	1000
250	250	1000
250	250	1000

(c)

Figure 4-11 : Three partial shading situations

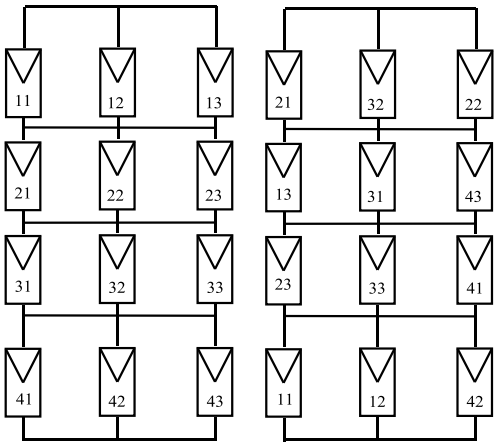

(a) (b)

Figure 4-12: (a) TCT interconnection; (b) OTCT interconnection

4.7.2.1 Situation (a)

In this situation, OTCT interconnection does not cause the bypass diodes to be turned ON. This increases the generated power by 7.1 % when compared to those for SP or TCT, as shown in Table 4-4. Moreover, the P-V characteristic is smoother, as shown in Figure 4-12.

Table 4-4: Situation (a) simulation results

	Modules' powers at $MPPA_a$ (W)			$MPPA_a$ (W)	PR_a	Power change w.r.t. SP (%)
SP &TCT	85	85	85	491.4	0.77	---
	85	85	85			
	-3.1	-3.1	-3.1			
	-3.1	-3.1	-3.1			
OTCT	66.7	66.7	83.5	526.4	0.83	+7.1
	66.7	66.7	83.5			
	19.1	13.6	13.6			
	13.6	19.1	13.6			

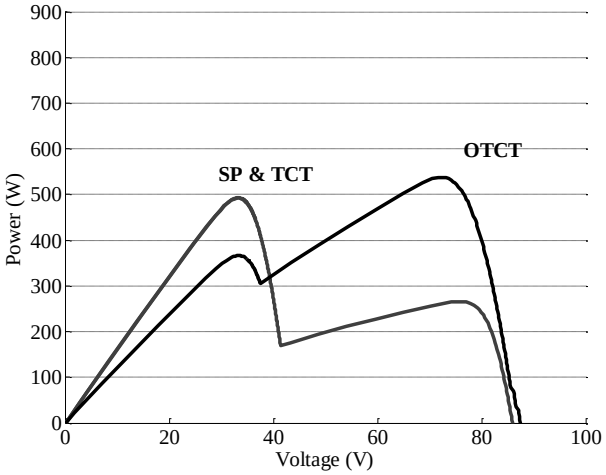

Figure 4-13 : situation (a) interconnections' P-V characteristics

4.7.2.2 Situation (b)

In this situation, the OTCT interconnection increased the performance ratio from 0.91 to 0.95, as shown in Table 4-5, and smoothed the P-V characteristic, as shown in Figure 4-13. This improvement comes from keeping the bypass diodes OFF.

Figure 4-14 Situation (b), simulation results

	Modules' powers at $MPPA_b$ (W)			$MPPA_b$ (W)	PR_b	Power change w.r.t. SP (%)
SP & TCT	85	85	85	755.7	0.91	---
	85	85	85			
	85	85	85			
	-3.1	-3.1	-3.1			
OTCT	84.8	84.8	84.8	783.9	0.95	+3.7
	72.2	72.2	84.8			
	84.8	72.2	84.8			
	19.5	19. 5	19.5			

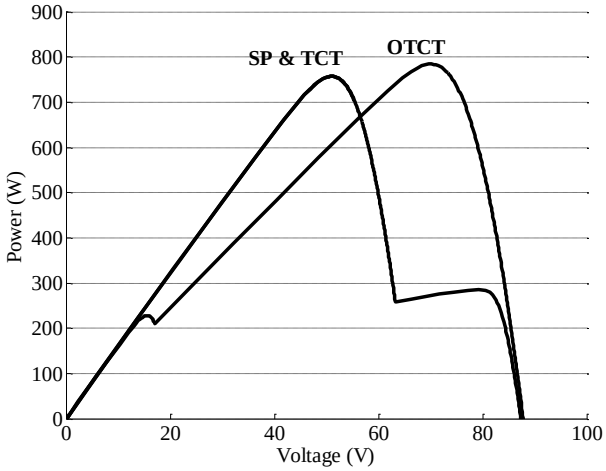

Figure 4-15 : situation (b) interconnections' P-V characteristics

4.7.2.3 Situation (c)

In this situation, the OTCT increased the coherence between the PV modules when compared to TCT or SP, as shown in Table 4-6. The increased coherence resulted in having a unity performance ratio for OTCT and increasing the generated power by 48 % when compared to SP. Moreover, the P-V characteristic has one peak only, as shown in Figure 4-14.

Table 4-5 Situation (c) simulation results

	Modules' powers at $MPPA_c$ (W)			$MPPA_c$ (W)	PR_c	Power change w.r.t. SP (%)
SP	26.1	26.1	85.1	510	0.67	---
	26.1	26.1	85.1			
	16.3	16.3	85.1			
	16.3	16.3	85.1			
TCT	51.1	51.1	51.1	549.6	0.72	+7.8
	51.1	51.1	51.1			
	19.1	19.1	83.3			
	19.1	19.1	83.3			
OTCT	85.1	85.1	85.1	759.2	1.00	+48.9
	85.1	85.1	85.1			
	19.6	19.6	85.1			
	19.6	19.6	85.1			

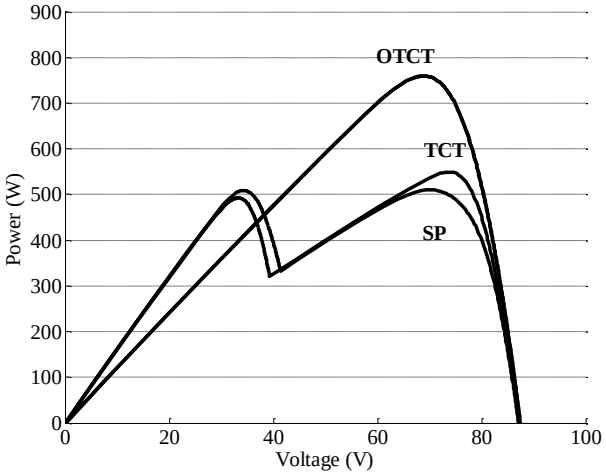

Figure 4-16 : situation (c) interconnections' P-V characteristics

From the previous situations and using (9), the OTCT interconnection increases the annual energy yield during partial shading by 17.8 % when compared to SP and by 15.2 % when compared to TCT. Moreover, using (4-8), (4-9) and (4-10), the PR during partial shading for OTCT increases to 0.93 from 0.79 for SP and 0.81 for TCT. The application examples presented in this section indicate that the OTCT interconnection results in an increase in the annual energy in the presence of partial shading; however, it will increase the complexity of the interconnection. The extent of increase in the complexity depends on the specific situation. It should be noted that the proposed mathematical model is general and gives the OTCT interconnection when the information on the shading pattern, irradiance levels and duration of each partial shading situation is provided.

4.8 Conclusion

This chapter proposed the Optimal-Total-Cross-Tied (OTCT) interconnection for photovoltaic arrays. As verified by a number of application case studies, this interconnection is capable of significantly reducing mismatch losses caused by easy-to-predict sources when compared to Series-Parallel (SP) or Total-Cross-Tied (TCT) interconnections, without using any switches or sensors. This reduction is a significant improvement in the design of photovoltaic structures, and is especially useful in the planning stage for large photovoltaic farms. The OTCT interconnection also results in a smoother array P-V characteristic with lower number of local maxima, thus simplifying the task of MPPT. Since the formulation of the optimization problem is general, the improvements are not restricted to the application case studies considered and are valid for any general condition. This work is

protected by the international patent number PCT/CA2011/000556. The next chapter considers difficult-to-predict sources of mismatch.

Chapter 5
Optimal Photovoltaic Array Reconfiguration to Reduce Partial Shading losses

5.1 Introduction

Sources of partial shading could be easy-to-predict sources such as nearby arrays and trees, or difficult-to-predict sources such as clouds, dust and snow. Unlike partial shading resulting from difficult-to-predict sources, partial shading caused by easy-to-predict sources can be reduced by selecting the proper array interconnection, as mentioned in the previous chapter. For example, partial shading from neighboring arrays in PV farms can be reduced by connecting the array in Optimal-Total-Cross-Tied (OTCT) interconnection.

The main goal of this chapter is to develop a mathematical formulation for the optimal PV array reconfiguration to reduce partial shading losses that come from difficult-to-predict sources. The second goal is to find the optimal solution for the optimization problem using a global optimization technique. This chapter is organized as follows: First, the mechanisms of partial shading losses are discussed. Then, a literature survey on techniques for reduction of partial shading losses is reported. Next, the reconfiguration problem and its optimal solution algorithm are presented. Finally, some applications for the proposed formulation are discussed, followed by conclusions and proposed future work.

5.2 Clouds Movement

The passage of clouds over a PV array is one of the main reasons for partial shading. There are two main cloud patterns. The puffy clouds that look like large cotton balls which are called cumulus clouds and the solid line of black clouds which are called squall lines. Cumulus clouds does not reduce the irradiance levels greatly; however they can cause the irradiance levels to fluctuate greatly [78-79]. Squall lines cause the largest variations in the irradiance levels and they can cause zero irradiance level [78-79], and thus, they lead to the worst-case scenario for partial shading; however, the speed of fluctuations is less than squall lines. The speed of fluctuations can range from few minutes to hours depending on the wind speed and the type and size of passing clouds [78-79].

5.3 Partial Shading Losses

Partial Shading (PS) causes power losses through different mechanisms, the most severe one being the incoherence of array's Maximum Power Point (MPP) with modules' MPPs. This means that the MPP operation of the array does not coincide with the MPP operations of the individual modules; therefore, the overall operation is not optimal. Another mechanism is turning bypass diodes ON, bypassing partially-shaded modules, although they might still be able to generate power. Moreover, turning these diodes ON creates losses due their ON-state resistances. PS could also cause reverse currents which make the reversed modules to act as loads, thus reducing the generation and increasing the thermal losses. In addition to the previous mechanisms, PS increases the probability of Maximum Power Point Tracker (MPPT) being misled to operate at local maxima which can add to the losses [5-9]. Different losses caused by PS are illustrated in Figure 5-1, where the maximum possible power under PS is the sum of the maximum powers of the individual modules when operating independently under the same irradiance levels dictated by array PS. The maximum possible power is less than the array's maximum power without partial shading. The difference is the shading losses which cannot be avoided.

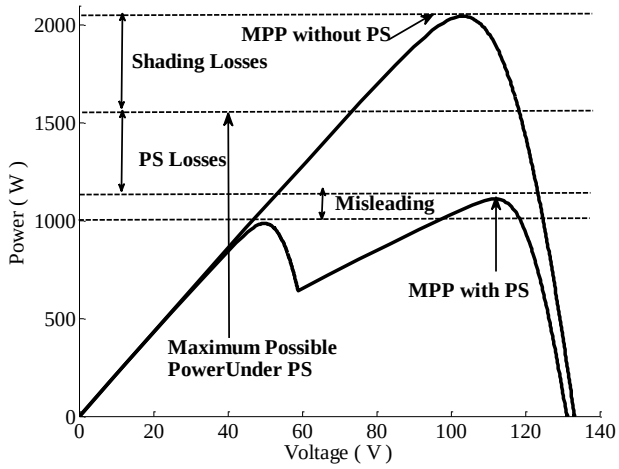

Figure 5-1: Shading, partial shading and misleading losses for a photovoltaic array

5.4 Partial Shading Loss Reduction

PS losses could be reduced by either passive or active techniques. Passive techniques use passive elements such as bypass diodes while active techniques use active elements such as solid-state switches. The most common passive technique uses bypass diodes across PV modules to reduce PS

losses. These diodes protect the modules from local heating (hot spots) and increase the overall power generation from the array under partial shading conditions. However, theses diodes do not allow the array to produce the maximum possible power under partial shading. Moreover, they increase the complexity of MPPT, as discussed earlier. Another passive technique is based on changing PV array interconnections. Active techniques for reducing partial shading losses could be grouped into the following main three categories:

5.4.1 Distributed MPPT

In this technique, each module or group of modules has its own MPPT, thus avoiding PS losses caused by the incoherence between the modules. Also, this technique avoids the installation of bypass diodes, thus avoiding the corresponding losses. Moreover, the MPPT detection is easier and does not require complicated algorithms. However, this technique requires additional components for each module or group of modules, such as DC-DC or DC-AC converters. Moreover, it requires more complicated control architectures.

5.4.2 Multi-level inverters

Multi-level inverter topologies such as diode-clamped, capacitor clamped and cascaded H-bridge have been used to reduce PS losses by independent voltage control of each module. These inverters reduce the device voltage stress as well as the ac output voltage harmonics. However, they require a complicated control algorithm to achieve operation at the optimal power point.

5.4.3 Photovoltaic array reconfiguration

The reconfigurable PV array was first proposed by Salameh et al. to start and operate permanent magnet dc motor coupled to volumetric water pump [43-44]. Then, it was proposed by [45] to start and accelerate electric cars using a number of PV modules. In [46], Sherif and Boutros proposed a reconfiguration scheme for PV modules using transistors as switches between cells. In [25], Nguyen and Lehman used reconfiguration inside PV arrays and proposed two reconfiguration algorithms. However, they did not propose any mathematical formulation for the optimal reconfiguration. They also proposed dividing the PV array into fixed and adaptive parts with a switching matrix between them. They used one column only as an adaptive part in order to reduce the number of sensors and switches, which can make the scheme ineffective if the shaded area is large. Moreover, they did not mention the necessary modifications in their algorithms to deal with higher number of reconfigurable columns. They tested the system under constant resistive load without MPPT. In [26, 47-48],

Velasco et al. used reconfiguration for grid connected PV arrays and proposed a mathematical formulation for it. However, the formulation is for a fully reconfigurable array only and it does not indicate directly the global optimal reconfiguration. Moreover, they proposed the irradiance equalization index as the difference between the maximum and the minimum average row irradiance levels in the array. They claimed that minimization of this index could result in an optimal reconfiguration. However, optimal reconfiguration requires that all the differences between row irradiance levels are minimized, as will be shown in this chapter. They proposed a solution algorithm that required an off-line determination of all possible configurations of the PV modules. Then, the best configuration for the current shading condition was found on-line. They tested the system using six PV modules and identified 15 possible configurations. Also, they found that nine PV modules will have 280 possible configurations. The number of possible configurations will increase for larger PV arrays and it will be very difficult to find the optimal configuration in a timely manner. It can be concluded that the proposed algorithm in [26, 47-48] is more suitable for small number of PV modules.

The formulation proposed is this chapter is intended to cover the shortfalls in the past work in the area. It can find directly the optimal reconfiguration if solved by a global optimization technique. Moreover, it is suitable for a fully reconfigurable or a partially reconfigurable array. In addition, it can be used for arrays with different number of modules per row. The solution algorithm proposed in this chapter ensures a global optimal reconfiguration.

5.5 Optimal PV Array Reconfiguration

By dynamically reconfiguring the connection of PV modules, the effect of irradiance level mismatch between PV modules can be minimized on the row level. For Total-Cross-Tied (TCT) interconnection, this can be seen as having one column of PV modules with equal or close-to-equal irradiance levels. The definition of irradiance level mismatch index is as follows:

Definition 1 "Irradiance level Mismatch Index IMI" is the sum of the squares of differences between normalized total irradiance levels of rows, as given by (5-1).

$$\mathrm{IMI} = 0.5 \sum_{i=1}^{m} \sum_{l=1}^{m} \left[\frac{\mathrm{IRR_i}}{G} - \frac{\mathrm{IRR_l}}{G} \right]^2 \qquad (5-1)$$

In (5-1), IRRi and IRRl are the total irradiance levels of rows i and l, respectively. Figure 5-2 shows an m × n PV array composed of two parts, a fixed part and a reconfigurable part. The objective is to

reconfigure the modules in the reconfigurable part in such a way that IMI is minimized. This requires defining an existence variable as follows.

Definition 2 "Existence Variable y_{iq}" is defined as a binary variable such that:

$$y_{iq} = \begin{cases} 1, & \text{if module q exists in row i} \\ 0, & \text{otherwise} \end{cases}$$

The objective function can therefore be formulated as follows.

$$\text{Minimize (IMI} = 0.5 \sum_{i=1}^{m} \sum_{l=1}^{m} \left[\frac{IRF_i}{G} + \sum_{q=1}^{mn_R} \frac{IRM_q y_{iq}}{G} - \frac{IRF_l}{G} - \sum_{q=1}^{mn_R} \frac{IRM_q y_{lq}}{G} \right]^2) \qquad (5-2)$$

In (5-2), the total normalized irradiance level of each row is represented by the summation of the normalized irradiance level of the fixed part $\frac{IRF_i}{G}$ and the normalized irradiance level of the reconfigurable part $\sum_{q=1}^{mn_R} \frac{IRM_q y_{iq}}{G}$. In (5-2), IRF_i represents the total irradiance level of the fixed part of row i, IRM_q represents the irradiance level of the reconfigurable module q, G is the reference irradiance level, m the total number of rows and n_R the total number of reconfigurable columns. The irradiance level of the reconfigurable part is found by the summation of irradiance levels of all modules that exist in the reconfigurable part. A module q will exist in the reconfigurable part if and only if y_{iq} is equal to one. Equations (5-3) and (5-4) give two logical constrains for the optimal reconfiguration problem. The first constrain described by (5-3) states that all reconfigurable modules should exist. This constraint is repeated $m \times n_R$ times. The second constraint described by (5-4) states that each reconfigurable part in each row will have n_R modules or less. This constraint is repeated m times. The inequality (5-4) could be changed to equality for exactly n_R modules per row.

$$\sum_{i=1}^{m} y_{iq} = 1 \qquad \forall q \qquad (5-3)$$

$$\sum_{q=1}^{m \times n_R} y_{iq} \leq n_R \qquad \forall i \qquad (5-4)$$

The previous optimization model can be used for fully- reconfigurable arrays if IRF_i is set to zero, or partially-reconfigurable arrays otherwise. Also, it can be used for different number of modules per row if (5-4) is an inequality constraint. The proposed model requires irradiance level data only and does not require any knowledge about the model of the PV modules.

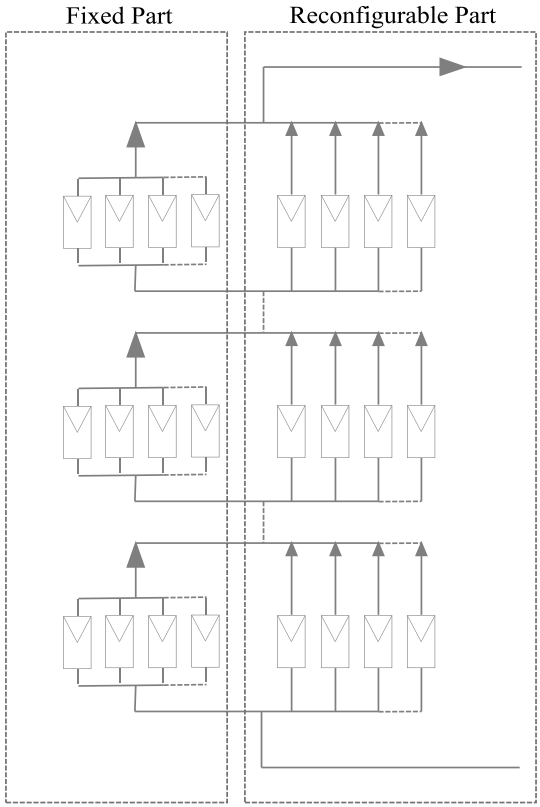

Figure 5-2: Reconfigurable PV array

5.6 Switches and Sensors Requirements

The proposed formulation requires a double-pole m-throw switch for each reconfigurable module as shown in Fig. 5-3. Therefore, the required total number of switches is $m \times n_R$. This number can be reduced by reducing the number of rows or the number of reconfigurable columns. The minimum number of rows is limited by the required voltage level from the array. However, the number of reconfigurable columns can be reduced by proper selection of the position of the reconfigurable columns. The users have the flexibility to select the number and the locations of reconfigurable columns according to their needs and according to the patterns of partial shading they have. Moreover, the users have the flexibility to select the number of modules per row according to their needs.

Irradiance levels can be measured by irradiance level sensors or estimated using voltage and current measurements. The cost of irradiance level sensors is much higher than those of voltage and current sensors. Therefore, it is proposed to use a voltage sensor for each row and a current sensor for each

module; then, the total number of sensors is m× (1+n_f+n_R). The irradiance level of each module IRM can be estimated by measuring its voltage VM and its current IM and substituting in (5-5) which requires the knowledge of module's parameters that could change by aging.

$$\mathrm{IRM} = \frac{\mathrm{G}}{\mathrm{I_{sc}}}\left[\mathrm{I_0}\left(\mathrm{e}^{\frac{\frac{\mathrm{VM}}{\mathrm{N_s}}+\mathrm{R_s IM}}{\mathrm{V_T}}} - 1\right) + \frac{\frac{\mathrm{VM}}{\mathrm{N_s}} + \mathrm{R_s IM}}{\mathrm{R_P}} + \mathrm{IM}\right] \quad (5-5)$$

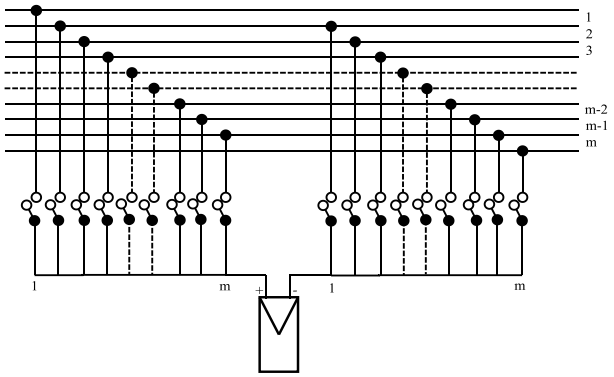

Figure 5-3: A reconfigurable PV module requires a double-pole m-throw switch

5.7 Optimization Algorithm and Simulation Model

The optimal reconfiguration problem is a Mixed Integer Quadratic Programming (MIQP) problem with $m^2 \times n_R$ binary variables. MIQP problems are NP-hard problems and their computational complexity is exponential in the number of binary variables [49]. However, a lot of efforts have been made to develop real time solvers for these problems [50-52]. These solvers usually use Branch and Bound (BB) algorithm. These solvers usually solve the problem in the range of 100 milliseconds [50-52] which is much faster than the speed of fluctuation of irradiance levels which ranges from few minutes to hours [78].

5.8 Performance Ratio and Economical Evaluation Method

The array's overall Performance Ratio (PR) given by (5-6) normalizes the effect of partial shading losses based on the rated output dc power P_{dc}, and allows comparison between arrays of different sizes under different irradiance conditions HA [13].

$$\mathrm{PR} = \frac{\mathrm{EA}}{\mathrm{HA}} \times \frac{\mathrm{G}}{\mathrm{P_{dc}}} \quad (5-6)$$

The array's energy production under partial shading (EA) and its in-plane irradiance level during partial shading (HA) used in (5-6) are given by (5-7) and (5-8) respectively.

$$\mathrm{EA} = \mathrm{PA} \times \mathrm{t} \qquad (5-7)$$

$$\mathrm{HA} = \mathrm{IRA} \times \mathrm{t} \qquad (5-8)$$

where t is the duration of partial shading. The array's PR can be found as follows:

$$\mathrm{PR} = \frac{\mathrm{PA} \times \mathrm{t}}{\mathrm{IRA} \times \mathrm{t}} \times \frac{\mathrm{G}}{\mathrm{P_{dc}}} = \frac{\mathrm{PA}}{\mathrm{IRA}} \times \frac{\mathrm{G}}{\mathrm{P_{dc}}} \quad (5-9)$$

The Revenue Present Value (RPV) from recovering partial shading energy losses is given by (5-10), where F is the inflation rate, D is the discount rate, $\Delta \mathrm{PA}_{gk}$ is the change in array output dc power due to reconfiguration, t_{gk} is the duration of partial shading situation, CE is the negotiated contract price, Y is the array life time in years, N is the number of partial shading situations per year, g is partial shading situation index and k is year index. The Cost Present Value (CPV) is given by (5-11), where N_{sw} is the total number of switches, N_I is the total number of current sensors, N_V is the total number of voltage sensors, a is the switch cost, b is the current sensor cost, c the voltage sensor cost and d cost of controller. The Net Present Value is given in (5-12).

$$RPV = \sum_{k=1}^{Y} \sum_{g=1}^{N} \left[\frac{(\Delta PA_{gk} t_{gk})(1+F)^{k-1}}{(1+D)^{k}} \right] CE \quad (5-10)$$

$$CPV = aN_{SW} + bN_I + cN_V + d \quad (5-11)$$

$$NPV = RPV - CPV \quad (5-12)$$

5.9 Application Examples

The following application examples consider a 6 × 4 PV array, where the first and third columns are fixed and the second and fourth columns are reconfigurable to form a Half-Reconfigurable Photovoltaic Array (HRPVA). This reduces the required number of switches to half of what was proposed in [26, 47-48] for Fully-Reconfigurable PhotoVoltaic Array (FRPVA). However, this results in reduction of the generated power in some partial shading situations.

The reconfiguration problem is modeled in GAMS and solved using Basic Open-source Non-linear Mixed INteger (BONMIN) solver [53]. This solver is set up to implement BB algorithm. A simulation model is needed to compare HRPVA, FRPVA and TCT arrays. The simulation model is built in MATLAB/SIMULINK environment. This model is based on the single diode model for PV

modules described by (4-5) and shown in Fig. 4-3. The PV array is constructed from the interconnection of PV modules in HRPVA, FRPVA or TCT. A bypass diode is connected across each PV module and no reverse current blocking diodes are modeled. The PV module data is given in Appendix A. The optimization software is installed on a PC, which has an Intel Core 2 Due processor with a speed of 1.8 GHz and a RAM memory of 1 GB. Performance ratio and irradiance mismatch index are calculated for each application example to give an indication of partial shading losses. Moreover, the processing time required to solve the optimization problem in each example is given.

5.9.1 Application Example 1: Single-Row Shading

The PS situations shown in Figure 5-4 are applied to TCT, HRPVA and FRPVA arrays, where the numbers indicate modules' irradiance levels in W/m^2. It should be noted that the MPP for the modules receiving 1000 W/m^2 irradiance level is 85 W and for those receiving 500 W/m^2 is 42.2 W. The FRPVA has increased the generated power by 8.5 % when compared to TCT. This increase comes from preventing bypass diodes from turning ON, which would short the 500 W/m^2 modules, as shown in Table 1. The HRPVA has increased the generated power by only 0.5 %. However, the Power-Voltage (P-V) characteristic is smoother than that of TCT, as shown in Figure 5-5, which reduces the probability of misleading the MPPT. The optimization processing time is 13.6 sec for HRPVA and 18.5 sec for FRPVA.

1000	1000	1000	1000
1000	1000	1000	1000
1000	1000	1000	1000
1000	1000	1000	1000
1000	1000	1000	1000
500	500	500	500

(a)

1000	1000	1000	500
1000	1000	1000	1000
1000	1000	1000	1000
1000	1000	1000	1000
1000	500	1000	1000
500	1000	500	1000

(b)

1000	1000	1000	500
1000	1000	1000	1000
1000	1000	1000	1000
1000	1000	500	1000
1000	500	1000	1000
500	1000	1000	1000

(c)

Figure 5-4: Application Example 1: (a) TCT irradiance levels; (b) HRPVA effective irradiance levels; (c) FRPVA effective irradiance levels

Table 5-1 Application Example 1: Array and modules' powers

	Modules' powers at Array's MPP (W)				Array's MPP (W)	PR	IMI	Power change w.r.t. TCT (%)	T (s)
TCT	85	85	85	85	1691	0.9	20	--	-
	85	85	85	85					
	85	85	85	85					
	85	85	85	85					
	85	85	85	85					
	-3.1	-3.1	-3.1	-3.1					
HRPVA	81.5	81.5	81.5	41.5	1700	0.91	5	+0.5	13.6
	74.4	74.4	74.4	74.4					
	74.4	74.4	74.4	74.4					
	74.4	74.4	74.4	74.4					
	81.5	41.5	81.5	81.5					
	38.2	78.4	38.2	78.4					
FRPVA	84.9	84.9	84.9	41.8	1834	0.98	2	+8.5	18.5
	81.1	81.1	81.1	81.1					
	81.1	81.1	81.1	81.1					
	84.9	84.9	41.8	84.9					
	84.9	41.8	84.9	84.9					
	41.8	84.9	84.9	84.9					

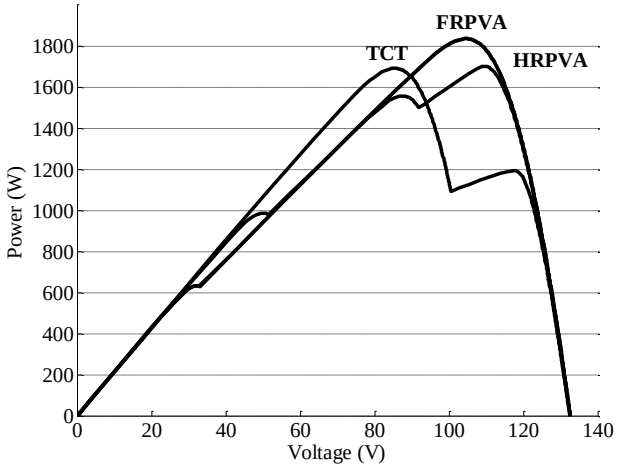

Figure 5-5: Application Example 1: Arrays' P-V characteristics

5.9.2 Application Example 2: Double-Row Shading

In this situation, the effective irradiance levels seen by each array is shown in Figure 5-6. The HRPVA and FPVA have reduced partial shading losses caused by turning ON of bypass diodes across the 500 W/m^2 modules, as shown in Table 5-2, thus increasing the generated power by 21.8 %, when compared to that for TCT. This is also reflected in the performance ratio which has increased

from 0.787 to 0.959 and the irradiance mismatch index which has decreased from 32 to 2. Moreover, the P-V characteristics of the reconfigurable arrays are smoother than that of TCT, as shown in Figure 5-7, thus reducing the probability of misleading the MPPT. The optimization processing time is 1.9 sec for HRPVA and 21.7 sec for FRPVA.

1000	1000	1000	1000
1000	1000	1000	1000
1000	1000	1000	1000
1000	1000	1000	1000
500	500	500	500
500	500	500	500

(a)

1000	1000	1000	500
1000	500	1000	1000
1000	500	1000	1000
1000	1000	1000	500
500	1000	500	1000
500	1000	500	1000

(b)

1000	1000	500	1000
1000	500	1000	1000
1000	500	1000	500
500	1000	1000	1000
500	1000	500	1000
1000	500	1000	1000

(c)

Figure 5-6: Application Example 2: (a) Applied irradiance levels; (b) HRPVA effective irradiance levels; (c) FRPVA effective irradiance levels

Table 5-2 Application Example 2: Array and modules' powers

	Modules' powers at Array's MPP (W)				Array's MPP (W)	PR	IMI	Power change w.r.t. TCT (%)	T (s)
TCT	85	85	85	85	1338	0.787	32	--	-
	85	85	85	85					
	85	85	85	85					
	85	85	85	85					
	-3.1	-3.1	-3.1	-3.1					
	-3.1	-3.1	-3.1	-3.1					
HRPVA	80.8	80.8	80.8	41.2	1630	0.959	2	+21.8	1.9
	80.8	41.2	80.8	80.8					
	80.8	41.2	80.8	80.8					
	80.8	80.8	80.8	41.2					
	40.6	83.1	40.6	83.1					
	40.6	83.1	40.6	83.1					
FRPVA	80.8	80.8	41.2	80.8	1630	0.959	2	+21.8	21.7
	80.8	41.2	80.8	80.8					
	83.1	40.6	83.1	40.6					
	41.2	80.8	80.8	80.8					
	40.6	83.1	40.6	83.1					
	80.8	41.2	80.8	80.8					

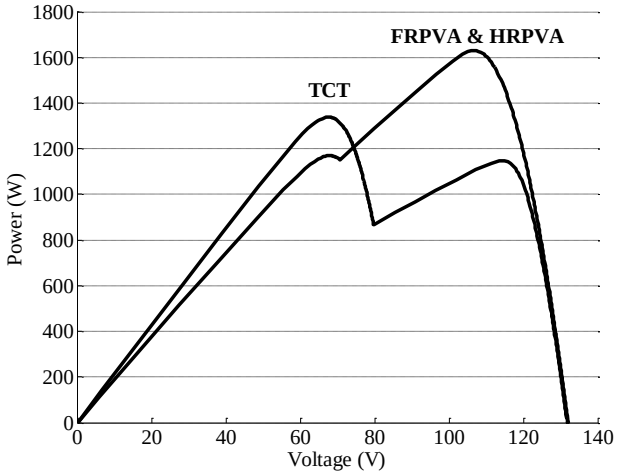

Figure 5-7: Application Example 2: Arrays' P-V characteristics

5.9.3 Application Example 3: Quarter-Array Shading

The irradiance levels shown in Figure 5-8 are applied to different PV arrays. The HRPVA and the FRPVA have reduced partial shading losses caused by incoherence between the modules' MPPs and the array's MPP, as shown in Table 5-3. The 1000 W/m^2 module is now able to produce 85 W instead of 73.1 W and the 500 W/m^2 module is able to produce 42.5 W instead of 41.2 W, increasing the overall array power production by 9.6 %, when compared to that for TCT. The reconfigurable arrays have a unity performance ratio and zero irradiance mismatch index. The P-V characteristics of the reconfigurable arrays are smoother than that of TCT, as shown in Figure 5-9, which simplifies the task of MPPT algorithm. The optimization processing time is 0.7 sec for HRPVA and 1.6 sec for FRPVA.

1000	1000	1000	1000
1000	1000	1000	1000
1000	1000	1000	1000
500	500	1000	1000
500	500	1000	1000
500	500	1000	1000

(a)

1000	500	1000	1000
1000	500	1000	1000
1000	500	1000	1000
500	1000	1000	1000
500	1000	1000	1000
500	1000	1000	1000

(b)

1000	1000	500	1000
1000	500	1000	1000
1000	1000	1000	500
500	1000	1000	1000
1000	1000	500	1000
1000	500	1000	1000

(c)

Figure 5-8: Application Example 3: (a) Applied irradiance levels; (b) RPVA effective irradiance levels ; (c) FRPVA effective irradiance levels

Table 5-3 Application Example 3: Array and modules' powers

	Modules' powers at Array's MPP (W)				Array's MPP (W)	PR	IMI	Power change w.r.t. TCT (%)	T (s)
TCT	73.1	73.1	73.1	73.1	1630	0.913	9	--	-
	73.1	73.1	73.1	73.1					
	73.1	73.1	73.1	73.1					
	41.2	41.2	84.1	84.1					
	41.2	41.2	84.1	84.1					
	41.2	41.2	84.1	84.1					
HRPVA	85	42.5	85	85	1786	1.000	0.00	+9.6	0.7
	85	42.5	85	85					
	85	42.5	85	85					
	42.5	85	85	85					
	42.5	85	85	85					
	42.5	85	85	85					
FRPVA	85	85	42.5	85	1786	1.000	0.00	+9.6	1.6
	85	42.5	85	85					
	85	85	85	42.5					
	42.5	85	85	85					
	85	85	42.5	85					
	85	42.5	85	85					

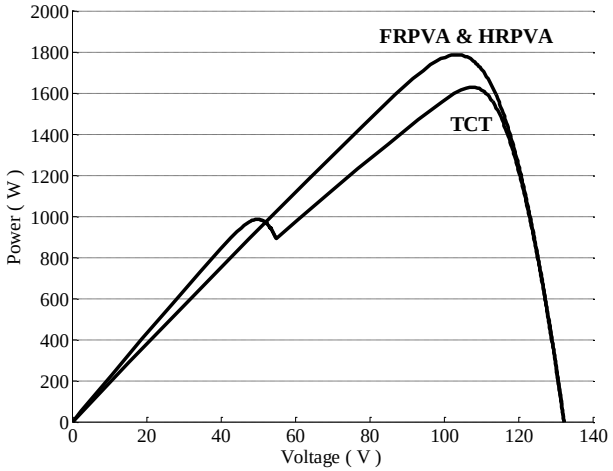

Figure 5-9 : Application Example 3: Arrays' P-V characteristics

5.9.4 Application Example 4: Oblique Shading

In this application, oblique shading is imposed on the three arrays, as shown in Figure 5-10. The reconfigurable arrays have increased the coherence between the modules' MPPs and the array's MPP which has increased the generated power by 23.3 % for FRPVA and by 15.7 % for HRPVA, as given

in Table 5-4 and shown in Figure 5-11. The optimization processing time is 7.1 sec for HRPVA and 1.6 sec for FRPVA.

1000	1000	1000	1000
1000	1000	1000	1000
1000	1000	1000	1000
500	1000	1000	1000
500	500	1000	1000
500	500	500	1000

(a)

1000	500	1000	1000
1000	1000	1000	1000
1000	500	1000	1000
500	1000	1000	1000
500	1000	1000	1000
500	1000	500	1000

(b)

1000	1000	500	1000
500	1000	1000	1000
1000	500	1000	1000
1000	1000	500	1000
1000	500	1000	1000
1000	500	500	1000

(c)

Figure 5-10: Application Example 4: (a) Applied irradiance levels; (b) RPVA effective irradiance levels ; (c) FRPVA effective irradiance levels

Table 5-4 Application Example 4: Array and modules' powers

	Modules' powers at Array's MPP (W)				Array's MPP (W)	PR	IMI	Power change w.r.t. TCT (%)	T (s)
TCT	63.8	63.8	63.8	63.8	1449	0.81	12	--	-
	63.8	63.8	63.8	63.8					
	63.8	63.8	63.8	63.8					
	36.5	71	71	71					
	40.7	40.7	79.4	79.4					
	38.2	38.2	38.2	78.3					
HRPVA	81.4	41.5	81.4	81.4	1677	0.94	3	+15.7	7.1
	74.3	74.3	74.3	74.3					
	81.4	41.5	81.4	81.4					
	41.5	81.4	81.4	81.4					
	41.5	81.4	81.4	81.4					
	38.7	79.5	38.7	79.5					
FRPVA	85	85	42.5	85	1786	1.000	0.00	+23.3	1.6
	42.5	85	85	85					
	85	42.5	85	85					
	85	85	42.5	85					
	85	42.5	85	85					
	85	42.5	85	85					

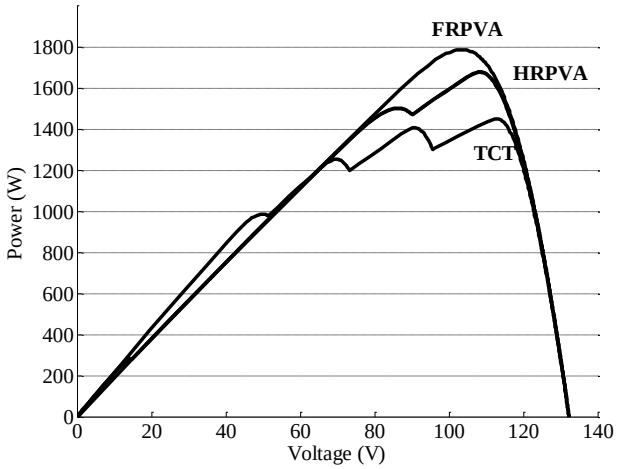

Figure 5-11: Application Example 4: Arrays' P-V characteristics

5.10 Economical Evaluation of the Application Examples

The 6×4 PV array used in the previous examples is assumed to be installed in Ontario with a total lifetime of 20 years. The energy sale price of PV in Ontario is $0.443/kWh for PV farms and $ 0.802/kWh for BIPV [3]. The inflation rate is assumed to be 4 % and the discount rate is assumed to be 8 % [74]. The full reconfigurable array uses 144 single-pole single-throw switches and the half reconfigurable array uses 72 switches. Both of them use 24 hall-effect current sensors, 6 resistive voltage divider, as voltage sensors, and one microcontroller. Based on the array voltage and current ratings, it was found that a single-pole single-throw switch costs $5, a hall effect current sensor costs $10, a resistive voltage divider costs $2 and the microcontroller costs $20 in scale production[73]. Also, it is assumed that the duration of partial shading is 10 % of the year (i.e., 0.1 × 8760 hrs = 876 hrs) and the four partial shading situations are equal in duration (i.e., 219 hrs each). Table 5-5 shows the results of the economical evaluation. The results show that the FRPVA and HRPVA used in the previous case studies are economically feasible for both BIPV and PV farm. However, this does not include the value of usage of the existing hardware for other functions such as series arc fault detection.

Table 5-5 Economical evaluation results

	FRPVA	HRPVA
RPV for PV farms	$1192.9	$880.4
RPV for BIPV	$2159.24	$1593.8
CPV	$992	$632
NPV for PV farms	$200.9	$248
NPV for BIPV	$1167.24	$961.8

5.11 Conclusion

In this chapter, a mathematical formulation for photovoltaic array reconfiguration as a Mixed Integer Quadratic Programming problem was proposed. This formulation can be used for a fully reconfigurable or a partially reconfigurable array. Moreover, it can be used for non-equal number of modules per row. It was shown that the application of the proposed reconfiguration concept can result in considerable reduction in partial shading losses, thus increasing the generated output power of arrays. A useful byproduct is the smoother P-V characteristic for the array, making the MPPT task much simpler. A method of economical evaluation for the proposed technology is presented and used in a specific case study in which reconfiguration showed economic feasibility. The intellectual property of some of the material presented in this chapter is protected by the international patent number PCT/CA2011/000809

Chapter 6

Series Arc Fault Detection in Total-Cross-Tied Photovoltaic Arrays

6.1 Introduction

PV systems are composed of modules, wires, connectors, diodes, junction boxes and inverters. These elements are usually operated at high DC voltages and are installed outdoors. These elements are subjected to animal bites, weather conditions and aging which can deteriorate their insulation. Moreover, the interconnection between these elements may become loose due to bad installation, weather conditions or aging. The deterioration of insulation and the loose interconnections are the main sources of faults in PV systems. Insulation deterioration can result in a ground fault if the current finds a path to ground. The loose interconnections can result in a series arc fault which is very difficult to detect and isolate. Moreover, if the deterioration is happening at two points that are physically close, this can result in a parallel arc fault, even though this rarely happens.

In 1984, the Sacramento Municipal Utility district started the operation of a 1 MW PV farm [54]. During start up, a fault occurred in the array field that led to a fire and a repair cost of around $58k. Through investigation, it was found that damaged insulation at two points had caused a double ground fault. As a result of this incidence and several other incidences, ground fault protection has become a must in every PV installation according to the American National Electric Code (NEC) [55]. Similar to ground faults, arc faults have caused damages to arrays and profit loss in many PV installations in different countries around the world [5]-[8]. Therefore, NEC has added article 690.11 in 2011 to require an arc fault protection. The focus of the article is on series arc faults for a system operating at 80V or greater. It requires automatic disconnection of the inverter or the faulted component upon detection of fault and the manual restoration of the disconnected element after clearing the fault [56]. This chapter proposes a novel series arc fault detection algorithm in compliance with the NEC standard.

Fault detection of PV arrays can be performed by visual inspection, thermal imaging with infrared camera or electrical measurements. Visual and thermal imaging methods require inspection by an experienced worker which can take a long time for a large PV farm. Electrical measurements can be much faster and more accurate than visual inspection and thermal imaging. The first proposed electrical method [57] was to measure the MPP voltage of the PV array to detect open circuit and short circuit faults. This method cannot discriminate between partial shading of the array and a fault

inside the array; also, it cannot detect the faulty module within the array. Measuring the array I-V characteristic and comparing it with a simulated I-V characteristic was proposed by [57]. This method requires an accurate model for the PV array and accurate measurements of irradiance and temperature for each module. This method can detect the faulty array but cannot detect the faulty module and cannot discriminate between a fault and partial shading. Earth Capacitance Measurement (ECM) was proposed by [58] for open circuit faults only. This method is based on the fact that the value of earth capacitance is independent of the irradiance level. ECM is used at the string level and cannot be used on the array level. Time Domain Reflectometry (TDR) is compared with ECM for increased contact resistance fault in [59]. In TDR, a signal is send to the PV string and is compared with the reflected signal. This comparison will give information about the type and location of fault. TDR is affected by installation circumstances such as wiring, module types and mounting materials. This means that the characteristics of the string should be measured directly after installation and after any change in string components or connections. Moreover, this method requires a signal generator which adds to the cost. Arc Fault Detectors (AFDs) are proposed to be installed at the terminals of the inverter or their functionality can be incorporated within the inverter [60]-[61]. These detectors sense the voltage and/or current at the terminals of the inverter and detect the presence of certain AC harmonics that corresponds to the fault. Upon fault detection, AFDs send a command signal to the main DC switch to disconnect the array, thus interrupting the series arc faults. The accuracy of AFDs in detection and localization of faults can be greatly affected by electromagnetic interference, harmonics, system parameters and partial shading [60], [62]-[63]. Another approach for detecting arc faults is by using module-level arc fault detector to detect faults and de-energize the module during faults [7], [64]. This technique uses an AFD for each module which increases the overall cost. Moreover, it can suffer from crosstalk nuisance tripping [76] and it cannot discriminate between series and parallel arc faults [77] which can lead to false interruption of parallel arc fault by opining the main array switch. In [65], they used current and voltage measurement from each module to find the distance in the Current-Voltage (I-V) space between the faulty module and the healthy modules; then, the fault is detected according to a certain threshold distance. This approach is interesting; however, it uses a huge number of sensors and cannot discriminate between faults and partial shading. This chapter will present a simple, but effective, arc fault detection and interruption technique that can discriminate between series arc faults and partial shading, thus avoiding the unnecessary disconnection of the array during partial shading.

6.2 Series Arc Fault Detection

Series arc fault causes a reduction in the affected row voltage when compared to other rows voltages. The reason is that it adds the arc fault resistance to the existing series resistance thus reducing the row voltage. Therefore, series arc fault can be detected by detecting the decrease in the affected row voltage when compared to healthy rows in a TCT interconnected array. The problem in this method is that there is another phenomena that causes a reduction in the affected row voltage when compared to others, this phenomena is called partial shading. Partial shading means that some modules in the array are having different irradiance levels from the rest of the modules. Having less irradiance levels in some rows reduces the row voltages when compared to other rows which misleads the detection of series arc fault detection, thus causing a false tripping of the array. To overcome this problem, series arc fault should be discriminated from partial shading. The difference between series arc fault and partial shading is that series arc fault usually occurs at a single point in series with a single module; however, partial shading usually covers more than one module.

The Row Voltage Mismatch Index between row i and row l ($RVMI_{il}$) defined in (6-1) is proposed to detect series arc fault or partial shading.

$$RVMI_{il} = (VR_i - VR_l)^2 \quad \forall\, i, (l < i) \quad (6-1)$$

Where VRi and VRl are the voltages of rows i and l respectively. $RVMI_{il}$ can be considered as a vector of size $\frac{m(m-1)}{2}$, where m is the number of rows. During single series arc fault without any partial shading or during a single row partial shading without any series arc fault this vector will have m-1 non-zero elements. However, for partial shading that involves more than one row without any series arc fault, the number of non-zero elements will be greater than m-1. For example, for double row partial shading, the number of non-zero elements is 2(m-2). The formula for the Number of Non-Zero (NNZ) elements is given by (6-2), where NSH is the number of the partially shaded rows, NSF is number of rows having series arc fault and NNO is the number of rows with no partial shading or series arc faults. The summation of NSH, NSF and NNO is equal to m as shown in (6-3).

$$NNZ = N_{NO}N_{SF} + N_{NO}N_{SH} + N_{SF}N_{SH} \quad (6-2)$$

$$m = N_{NO} + N_{SH} + N_{SF} \quad (6-3)$$

The possibility of having two or more series arc faults concurrently in the same array is very rare. Therefore, partial shading and series arc faults can be discriminated from each other according to NNZ. If NNZ is equal to m-1, then the case is series arc fault or single row partial shading and If

NNZ is greater than m-1, then the case is partial shading. The usage of $RVMI_{il}$ and NNZ fails to discriminate between series arc fault and partial shading in case of single row partial shading. Moreover, it fails to detect series arc faults if it is occurring concurrently with partial shading.

In case of single series arc fault occurring concurrently with partial shading the Second Row Voltage Mismatch Index ($SRVMI_{kq}$) defined in (6-4) is proposed. Where, $RVMI_k$ and $RVMI_q$ are vectors of all non-zero elements of $RVMI_{il}$. The Second Number of Non-Zero (SNNZ) elements given in (6-5) is proposed to discriminate between series arc fault occurring concurrently with partial shading and pure uniform partial shading (all shaded rows have equal irradiance levels). If series arc faults and partial shading are occurring concurrently, then SNNZ is greater than zero. Otherwise, if uniform partial shading is occurring only, then all non-zero row voltage mismatch indices are equal to each other for uniform partial shading among the partially shaded rows. Therefore, the $SRVMI_r$ is equal to zero and SNNZ is equal to zero. The usage of SNNZ and $SRVMI_{kq}$ can lead to nuisance tripping upon non-uniform partial shading.

$$SRVMI_{kq} = \left(RVMI_k - RVMI_q\right)^2 \qquad \forall\, k, (q < k) \quad (6-4)$$

$$SNNZ = N_{NO}^2 N_{SH} N_{SF} + N_{NO} N_{SH} N_{SF}^2 + N_{NO} N_{SH}^2 N_{SF} \quad (6-5)$$

The fault detection algorithm can be selected according to the probability of occurrence of partial shading and series arc fault. For example if the probability of having series arc fault and partial shading concurrently is small, then NNZ can be used alone as in algorithm 1 shown in Figure 6-1 and therefore the array will not suffer from nuisance tripping upon non-uniform partial shading. However, if the probability of having series arc fault and partial shading concurrently is high, then NNZ and SNNZ are required to ensure safe operation as in algorithm 2 shown in Figure 6-2; however, this can cause the array to suffer from nuisance tripping upon non-uniform partial shading.

If the PV array is interconnected in Optimal Total Cross Tied (OTCT) interconnection [66] instead of TCT interconnection, then the proposed method can discriminate between series arc fault and partial shading even in the case of single row shading. Moreover, the probability of having uniform partial shading among shaded rows is higher. The reason is that in OTCT interconnection, the modules of the partially shaded row are distributed among different parallel circuits, thus making the irradiance levels of the shaded rows more uniform.

Figure 6-3 shows the connection diagram for voltage measurements. The array requires m voltage sensors for voltage measurements and a microcontroller for processing. Voltage sensors could be resistance dividers which are very cheap and reliable. Moreover, if the array is a reconfigurable array as in [72] then the fault detection functionality can be incorporated within the same reconfiguration hardware.

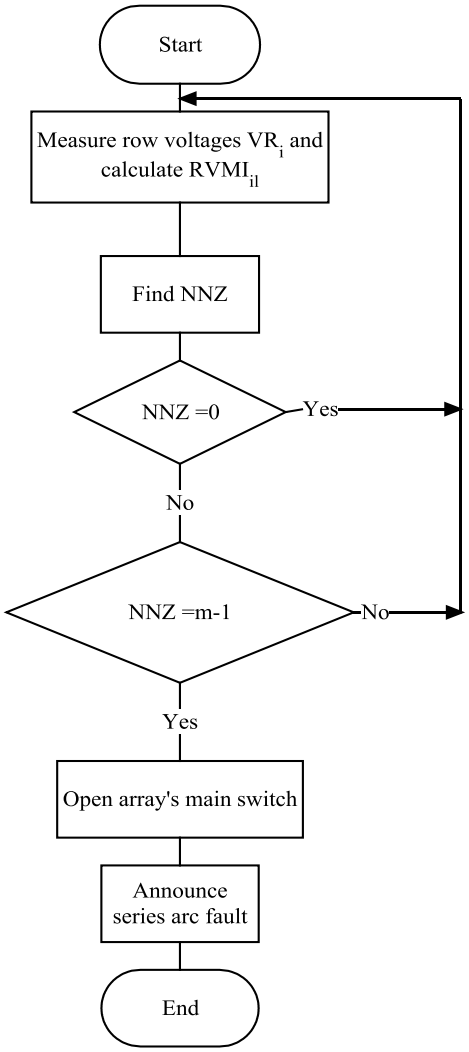

Figure 6-1: Algorithm 1 for detecting series arc fault when the probability of having series arc fault and partial shading concurrently is low.

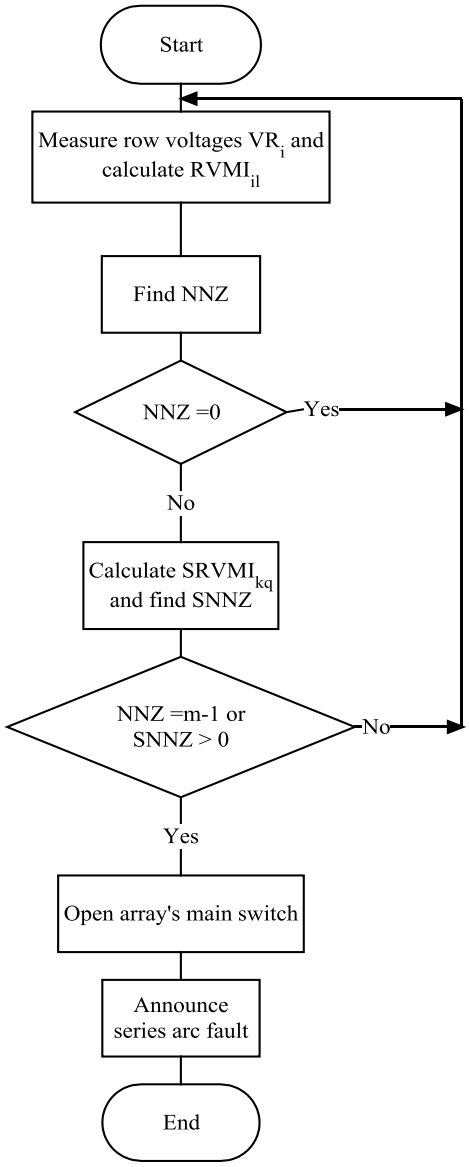

Figure 6-2: Algorithm 2 for detecting series arc fault when the probability of having series arc fault and partial shading concurrently is high.

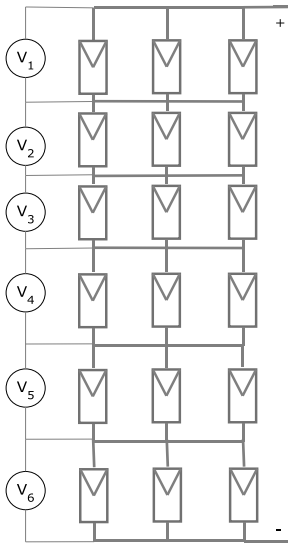

Figure 6-3: Connection diagram

6.3 Application Case Study

The following application case study is performed on two 6×4 arrays interconnected in TCT and OTCT and modeled in MATLAB/SIMULINK [75]. The building block of the system model is the PV cell, which is modeled by the single-diode equivalent circuit as given in Figure 3-1. The PV modules are modeled by the interconnection of a number of PV cells (module data are given in Appendix A). Each module has a bypass diode connected across its terminals. Finally, PV arrays are formed by PV module interconnections.

Table 6-1 shows the results of different case studies for TCT interconnected array. The first algorithm can detect series arc fault when happening alone without any partial shading. However, if series arc faults and partial shading are happening concurrently, it fails to detect series arc faults. The second algorithm can detect series arc faults in all the cases, even when it is occurring concurrently with partial shading. However, it is subjected to nuisance operation under non-uniform partial shading.

Table 6-2 shows the results for OTCT interconnection. OTCT interconnection avoids nuisance operation in case of single row shading. Moreover, it increase the uniformity of irradiance level, thus it reduces the probability of nuisance tripping for algorithm 2 during non-uniform partial shading.

Table 6-1: TCT case studies

Situation	NNZ	SNNZ	Algorithm 1	Algorithm 2
Normal operation	0	0	Normal Operation	Normal Operation
One row shading	5	0	Series Arc fault	Series Arc fault
Two rows uniform shading	8	0	Normal Operation	Normal Operation
Three rows uniform shading	9	0	Normal Operation	Normal Operation
Quarter array uniform shading	8	0	Normal Operation	Normal Operation
Single series arc fault	5	0	Series arc fault	Series arc fault
One row shading and one series arc fault in another row	9	24	Normal Operation	Series Arc fault
Two rows shading and one series arc fault in another row	11	36	Normal Operation	Series Arc fault
One row shading and series arc fault in the same row	5	0	Normal Operation	Series Arc fault
Two rows shading and series arc fault in one of the two rows	9	24	Normal Operation	Series Arc fault
Two rows non-uniform shading	9	24	Normal Operation	Series Arc fault

Table 6-2: OTCT case studies

Situation	NNZ	SNNZ	Algorithm 1	Algorithm 2
Normal operation	0	0	Normal Operation	Normal Operation
One row shading	8	0	Normal Operation	Normal Operation
Two rows uniform shading	8	0	Normal Operation	Normal Operation
Three rows uniform shading	0	0	Normal Operation	Normal Operation
Quarter array uniform shading	0	0	Normal Operation	Normal Operation
Single series arc fault	5	0	Series arc fault	Series arc fault
One row shading and one series arc fault in another row	9	24	Normal Operation	Series Arc fault
Two rows shading and one series arc fault in another row	11	36	Normal Operation	Series Arc fault
One row shading and series arc fault in the same row	11	36	Normal Operation	Series Arc fault
Two rows shading and series arc fault in one of the two rows	9	24	Normal Operation	Series Arc fault
Two rows non-uniform shading	Depends on irradiance levels	Depends on irradiance levels	Normal Operation or Series Arc fault	Normal Operation or Series Arc fault

6.4 Conclusion

Novel series arc fault detection algorithms that can discriminate between series arc faults and partial shading are proposed. The algorithms are based on the instantaneous measurements of row voltages in a Total-Cross-Tied (TCT) or Optimal-Total-Cross-Tied (OTCT) interconnected arrays. The first algorithm is used when the probability of having series arc faults and partial shading concurrently is low. The second algorithm is used to detect series arc faults when the probability of having series arc faults and partial shading concurrently is high. The second algorithm can detect series arc fault in all situations. However, it suffers from nuisance tripping during non-uniform partial shading.

Chapter 7
Conclusion

7.1 Summary

The main objectives of this thesis are to propose novel designs for photovoltaic arrays to reduce partial shading losses caused by easy- and difficult-to predict sources and to propose a novel algorithm for series arc fault detection.

The first proposed design is a passive design in which it finds the Optimal-Total-Cross-Tied (OTCT) interconnection for a number of partial shading situations. The OTCT interconnection reduces partial shading losses and smoothies the P-V characteristic, thus avoiding a complicated Maximum Power Point Tracking (MPPT) algorithm. Moreover, it reduces the possibility of turning ON bypass diodes; thus, they can be avoided in some situations. However, the OTCT interconnection increases the complexity of installation and it may require more labor time. Also, the OTCT interconnection may require additional wires to interconnect the modules.

The second proposed design is meant to dynamically reconfigure the photovoltaic array in real time to reduce partial shading losses. The reconfigurable array can reduce partial shading losses caused by difficult-to-predict sources such as clouds and snow. Moreover, it could reduce the land and installation requirements in large photovoltaic farms. However, the reconfigurable array requires switches, sensors and controllers which add to the installation cost.

The thesis proposed novel series arc fault detection algorithms. These algorithms can discriminate between series arc faults and partial shading, thus avoiding unnecessary interruption. The proposed algorithms are more suitable for the OTCT interconnection than the traditional Total-Cross-Tied (TCT) interconnection. Moreover, their functionality can be achieved using the same hardware used for the reconfigurable photovoltaic array. However, the algorithms assume the occurrence of single series arc fault at a time.

7.2 Contributions

The three main contributions of the thesis are as follows:

1- Optimal total-cross-tied interconnection for photovoltaic arrays to reduce mismatch losses

   The adoption of this interconnection in PV arrays can reduce significantly mismatch losses caused by easy-to-predict sources in building-integrated-photovoltaic systems and photovoltaic farms and it allows for using a simple MPPT and avoiding bypass diodes in some situations. Moreover, it can reduce the land and installation requirements of photovoltaic farms.

2- Optimal reconfiguration for photovoltaic arrays to reduce partial shading losses

   The Reconfigurable photovoltaic arrays can significantly reduce partial shading losses caused by difficult-to-predict sources and it can reduce the land and installation requirements in photovoltaic farms. The proposed formulation allows for partially reconfigurable arrays, thus reducing installation cost.

3- Series arc fault detection algorithm in total-cross-tied photovoltaic arrays

   A novel and simple arc fault detection algorithm for total-cross-tied and optimal-total-cross-tied arrays is proposed. This algorithm requires only row voltage measurements to discriminate between series arc faults and partial shading, thus avoiding the unnecessary disconnection of the array.

7.3 Future Work

The following items have been identified for future work based on the findings of this thesis:

1- Developing a simple method for making the connections in the OTCT interconnection to reduce installation time.

2- Developing an optimization model for the OTCT interconnection based on the double diode model.

3- Solving the optimization model for the OTCT interconnection using another algorithm such as genetic algorithm.

4- Modeling the change in irradiance levels caused by clouds, snow and dust using random variables and Monte Carlo simulation.

5- Performing economic analysis on the reconfigurable photovoltaic array to find the most economical number of reconfigurable columns based on site survey and historical partial shading data.

6- Building a prototype experiment for the reconfigurable PV array.

7- Testing the series arc fault detection algorithm in the field.

Appendix A

Shell PowerMax Solar Module (Ultra SQ85-P) Data

Number of series cells = 36

Nominal DC Power (P_{MPP}) = 85 W

Voltage at nominal power (V_{MPP}) = 17.2 V

Current at nominal power (I_{MPP}) = 4.95 A

Open circuit voltage (V_{OC}) = 22.2 V

Short circuit current (I_{SC}) = 5.45 A

Module efficiency (η) = 13.4 %

Temperature coefficient of P_{MPP} = -0.43 % /^{o}C

Temperature coefficient of V_{MPP} = -72.5 mV /^{o}C

Temperature coefficient of I_{MPP} = 1.4 mA /^{o}C

Temperature coefficient of V_{OC} = -64.5 mV /^{o}C

References

[1] "IEEE Recommended Criteria for Terrestrial Photovoltaic Power Systems," ANSI/IEEE Std 928-1986 , vol., no., pp.0_1, 1986.

[2] Total photovoltaic power installed in IEA PVPS countries. http://www.iea-pvps.org (Online November 2011).

[3] Feed in Tariff for Renewable Energy Projects in Ontario. (2009, Sep.). [Online]. Available: www.powerauthority.on.ca.

[4] http://www.enbridge.com/media/

[5] H. Haberlin and M. Real, "Arc Detector for Remote Detection of Dangerous Arcs on the DC Side of PV Plants", presented at the 22nd European Photovoltaic Solar Energy Conference, Milano, Italy, Sept. 2007.

[6] Strobl, C.; Meckler, P.; , "Arc Faults in Photovoltaic Systems," Electrical Contacts (HOLM), 2010 Proceedings of the 56th IEEE Holm Conference on , vol., no., pp.1-7, 4-7 Oct. 2010

[7] Schimpf, F.; Norum, L.E.; , "Recognition of electric arcing in the DC-wiring of photovoltaic systems," Telecommunications Energy Conference, 2009. INTELEC 2009. 31st International , vol., no., pp.1-6, 18-22 Oct. 2009.

[8] L. Ji, PV Fire: Experience and Studies, International Photovoltaic Reliability Workshop II, Tempe, AZ, July 31, 2009.

[9] The German Energy Society, "Planning and installing photovoltiac systems: a guide for installers, architects, and engineers,", 2nd ed., London. Sterling, VA: Earth scan., 2008, pp. 152-157.

[10] Ryan Duwain Warren," A feasibility study of stationary and dual axis tracking grid connected photovoltaic systems in the Upper Midwest" Ph.D thesis, Iowa State University, Iowa, 2008

[11] Optimisation of Design of Grid-Connected PV Systems under Danish Conditions. (2009, April).[Online]. www.solenergi.dk.

[12] Comparison of Storage Technologies for Distributed Resource Applications.(2003, Feb). [Online]. www.epri.com.

[13] B. Marion, J. Adelstein, K. Boyle , H. Hayden, B. Hammond, T.Fletcher, B.Canada, D.Narang, D.Shugar, H. Wenger, A.Kimber, L.Mitchell, G. Rich and T. Townsend, "Performance Parameters for Grid-connected PV Systems," 31st IEEE Photovoltaic specialists conference and Exhibition, Jan. 2005.

[14] Ueda, Y.; Kurokawa, K.; Itou, T.; Kitamura, K.; Miyamoto, Y.; Yokota, M.; Sugihara, H.; , "Performance Ratio and Yield Analysis of Grid Connected Clustered PV Systems in Japan," *Photovoltaic Energy Conversion, Conference Record of the 2006 IEEE 4th World Conference on* , vol.2, no., pp.2296-2299, May 2006.

[15] Performance Ratio for the 15 Largest PV Systems in the IEA PVPS Database. (2007,Aug.). [Online]. Available: http://www.iea-pvps.org.

[16] Spertino, F.; Akilimali, J.S.; , "Are Manufacturing I– V Mismatch and Reverse Currents Key Factors in Large Photovoltaic Arrays?," Industrial Electronics, IEEE Transactions on , vol.56, no.11, pp.4520-4531, Nov. 2009.

[17] N.D. Kaushika, Anil K. Rai, An investigation of mismatch losses in solar photovoltaic cell networks, Energy, Vol 32, Iss. 5, May 2007, pp. 755-759.

[18] M. Drif, P. J. Perez, J. Aguilera and J. D. Aguilar, "A new estimation method of irradiance on a partially shaded PV generator in grid-connected photovoltaic system," Renewable Energy, vol. 33, iss. 9 pp. 2048-2056, Feb. 2008.

[19] García, M., Vera, J. A., Marroyo, L., Lorenzo, E. and Pérez, M. (2009), Solar-tracking PV plants in Navarra: A 10 MW assessment. Progress in Photovoltaics: Research and Applications, April 2009.

[20] Femia, N.; Lisi, G.; Petrone, G.; Spagnuolo, G.; Vitelli, M.; , "Distributed Maximum Power Point Tracking of Photovoltaic Arrays: Novel Approach and System Analysis," Industrial Electronics, IEEE Transactions on , vol.55, no.7, pp.2610-2621, July 2008.

[21] Roman, E.; Alonso, R.; Ibanez, P.; Elorduizapatarietxe, S.; Goitia, D.; , "Intelligent PV Module for Grid-Connected PV Systems," Industrial Electronics, IEEE Transactions on , vol.53, no.4, pp.1066-1073, June 2006.

[22] Busquets-Monge, S.; Rocabert, J.; Rodriguez, P.; Alepuz, S.; Bordonau, J.; , "Multilevel Diode-Clamped Converter for Photovoltaic Generators With Independent Voltage Control of Each Solar Array,"Industrial Electronics, IEEE Transactions on , vol.55, no.7, pp.2713-2723, July 2008.

[23] Bratcu, A.I.; Munteanu, I.; Bacha, S.; Picault, D.; Raison, B.; , "Cascaded DC–DC Converter Photovoltaic Systems: Power Optimization Issues," Industrial Electronics, IEEE Transactions on , vol.58, no.2, pp.403-411, Feb. 2011.

[24] Lijun Gao; Dougal, R.A.; Shengyi Liu; Iotova, A.P.; , "Parallel-Connected Solar PV System to Address Partial and Rapidly Fluctuating Shadow Conditions," Industrial Electronics, IEEE Transactions on , vol.56, no.5, pp.1548-1556, May 2009.

[25] Dzung Nguyen and Lehman, B., "An Adaptive Solar Photovoltaic Array Using Model-Based Reconfiguration Algorithm," Industrial Electronics, IEEE Transactions on, vol. 55, no. 7, pp. 2644-2654, July 2008.

[26] Velasco-Quesada, G., Guinjoan-Gispert, F., Pique-Lopez, R., Roman-Lumbreras, M. and Conesa-Roca, A., "Electrical PV Array Reconfiguration Strategy for Energy Extraction Improvement in Grid-Connected PV Systems," Industrial Electronics, IEEE Transactions on, vol. 56, no. 11, pp. 4319-4331, Nov. 2009.

[27] Patel, H.; Agarwal, V., "MATLAB-Based Modeling to Study the Effects of Partial Shading on PV Array Characteristics," Energy Conversion, IEEE Transactions on , vol.23, no.1, pp.302-310, March 2008.

[28] Carannante, G.; Fraddanno, C.; Pagano, M.; Piegari, L.; , "Experimental Performance of MPPT Algorithm for Photovoltaic Sources Subject to Inhomogeneous Insolation," Industrial Electronics, IEEE Transactions on , vol.56, no.11, pp.4374-4380, Nov. 2009.

[29] Patel, H.; Agarwal, V.; , "Maximum Power Point Tracking Scheme for PV Systems Operating Under Partially Shaded Conditions," Industrial Electronics, IEEE Transactions on , vol.55, no.4, pp.1689-1698, April 2008.

[30] Peng Lei; Yaoyu Li; Seem, J.E.; , "Sequential ESC-Based Global MPPT Control for Photovoltaic Array With Variable Shading," Sustainable Energy, IEEE Transactions on , vol.2, no.3, pp.348-358, July 2011.

[31] Kadri, R.; Gaubert, J.-P.; Champenois, G.; , "An Improved Maximum Power Point Tracking for Photovoltaic Grid-Connected Inverter Based on Voltage-Oriented Control," Industrial Electronics, IEEE Transactions on , vol.58, no.1, pp.66-75, Jan. 2011.

[32] Qiang Mei; Mingwei Shan; Liying Liu; Guerrero, J.M.; , "A Novel Improved Variable Step-Size Incremental-Resistance MPPT Method for PV Systems," Industrial Electronics, IEEE Transactions on , vol.58, no.6, pp.2427-2434, June 2011.

[33] S. Silvestre, A. Boronat and A. Choudar "Study of bypass diodes configurtion on PV modules", Applied Energy , vol. 86, iss. 9, pp. 1632-1640, Sept. 2009.

[34] Acciari, G.; Graci, D.; La Scala, A.; , "Higher PV Module Efficiency by a Novel CBS Bypass," Power Electronics, IEEE Transactions on , vol.26, no.5, pp.1333-1336, May 2011.

[35] Kaushika, N.D.; Gautam, N.K.; "Energy yield simulations of interconnected solar PV arrays," Energy Conversion, IEEE Transactions on , vol.18, no.1, pp. 127- 134, Mar 2003.

[36] Picault, D.; Raison, B.; Bacha, S.; Aguilera, J.; De La Casa, J.; , "Changing photovoltaic array interconnections to reduce mismatch losses: a case study," Environment and Electrical Engineering (EEEIC), 2010 9th International Conference on , vol., no., pp.37-40, 16-19 May 2010.

[37] Di Dio, V.; La Cascia, D.; Miceli, R.; Rando, C.; , "A mathematical model to determine the electrical energy production in photovoltaic fields under mismatch effect," Clean Electrical Power, 2009 International Conference on , vol., no., pp.46-51, 9-11 June 2009

[38] Nalin K. Gautam, N. D. Kaushika, Reliability evaluation of solar photovoltaic arrays, Solar Energy, Vol. 72, Iss. 2, Feb. 2002, pp. 129-141.

[39] Kenneth H. Rosen, John G. Michales, Jonathan L. Gross, Jerrold W. Grossman, Douglas R. Shier “Hand book of Discrete and Combinatorial Mathematics”, 1st Edition, CRC Press, Florida, USA.

[40] Weinstock, D.; Appelbaum, J.; , "Shadow variation on photovoltaic collectors in a solar field," Electrical and Electronics Engineers in Israel, 2004. Proceedings. 2004 23rd IEEE Convention of , vol., no., pp. 354- 357, 6-7 Sept. 2004.

[41] J. Bany, J. Appelbaum, The effect of shading on the design of a field of solar collectors, Solar Cells, Volume 20, Issue 3, April 1987, Pages 201-228, ISSN 0379-6787.

[42] Dan Weinstock and Joseph Appelbaum, Optimal Solar Field Design of Stationary Collectors, J. Sol. Energy Eng. 126, 898 (2004).

[43] Z.M.Salameh and C.Liang. 'Optimum Switching Point for Array Reconfiguration Controllers'. IEEE 21st Photovoltaic Specialist Conference, 1990 (21st PVSEC). Vol. 2, pp. 971-976. Kissimmee (USA). May 1990.

[44] Z.M.Salameh and F.Dagher. 'The Effect of Electrical Array Reconfiguration on the Performance of a PV-Powered Volumetric Water Pump'. IEEE Transactions on Energy Conversions. Vol. 5, Iss. 2, pp. 653-658. December 1990.

[45] Y.Auttawaitkul, B.Pungsiri, K.Chammongthai and M.Okuda. 'A Method of Appropriate Electric Array Reconfiguration Management for Photovoltaic Powered Car'. The 1998 IEEE Asia-Pacific Conference on Circuits and Systems (APCCAS 98). Pp.: 201-204. Chiang (Thailand), November 1998.

[46] Raed A. Sherif and Karim S. Boutros “Solar Module Array with Reconfigurable Tile,” Patent No.: US 6,350,944 B1, Feb. 26, 2002.

[47] G. Velasco, J.J. Negroni, F. Guinjoan and R. Piqué. ‘Energy Generation in PV Grid-Connected Systems: A Comparative Study Depending on the PV Generator Configuration’. IEEE International Symposium on Industrial Electronics, 2005. (ISIE 05). Vol. 3, páginas 1025 - 1030. Dubrovnik (Croatia), June 2005.

[48] G. Velasco, J.J. Negroni, F. Guinjoan and R. Piqué. ‘Grid-Connected PV Systems Energy Extraction Improvement by means of an Electric Array Reconfiguration (EAR) Strategy: Operating Principle and Experimental Results’. IEEE 39th Power Electronics Specialists Conference, 2008. (PESC 08). Rhodes (Greece), June 2008.

[49] Daniel Axehill, “Applications of Integer Quadratic Programming in Control and Communication,” Linköping Studies in Science and Technology, thesis no. 1218, pp. 9-45, 2005.

[50] Shimai, Y.; Tani, J.; Noguchi, H.; Kawaguchi, H.; Yoshimoto, M.; , "FPGA implementation of mixed integer quadratic programming solver for mobile robot control," Field-Programmable Technology, 2009. FPT 2009. International Conference on , vol., no., pp.447-450, 9-11 Dec. 2009.

[51] Noguchi, H.; Tani, J.; Shimai, Y.; Nishino, M.; Izumi, S.; Kawaguchi, H.; Yoshimoto, M.; , "A 34.7-mW quad-core MIQP solver processor for robot control," Custom Integrated Circuits Conference (CICC), 2010 IEEE , vol., no., pp.1-4, 19-22 Sept. 2010.

[52] Nishino, M.; Noguchi, H.; Shimai, Y.; Izumi, S.; Kawaguchi, H.; Yoshimoto, M.; , "A 75-variable MIQP solver processor for real-time autonomous robot control," System Integration (SII), 2011 IEEE/SICE International Symposium on , vol., no., pp.469-472, 20-22 Dec. 2011

[53] GAMS Distribution 23.0, “A user’s guide,” GAMS Development Corporation, 2009.

[54] Chirone, L.; Califano, F.P.; Moschella, U.; Rocca, U.; , "Fault finding in a 1 MW photovoltaic plant by reflectometry," Photovoltaic Energy Conversion, 1994., Conference Record of the Twenty Fourth. IEEE Photovoltaic Specialists Conference - 1994, 1994 IEEE First World Conference on , vol.1, no., pp.846-849 vol.1, 5-9 Dec 1994.

[55] Bower, W.; Wiles, J.; , "Investigation of ground-fault protection devices for photovoltaic power system applications," Photovoltaic Specialists Conference, 2000. Conference Record of the Twenty-Eighth IEEE , vol., no., pp.1378-1383, 2000.

[56] Bower, W; Kuszmaul, S; Johnson, J; Strauch, J”Codes and Standerds for PV Arc Fault Detection and Mitigation”, “Solar Power International Conference”, Los Angeles, CA, 13 Oct, 2010.

[57] Stellbogen, D.; , "Use of PV circuit simulation for fault detection in PV array fields ," Photovoltaic Specialists Conference, 1993., Conference Record of the Twenty Third IEEE , vol., no., pp.1302-1307, 10-14 May 1993.

[58] Takumi Takashima, Junji Yamaguchi and Masayoshi Ishida, "Disconnection detection Using Earth Capacitance Measurements in Photovoltaic Modules String" Progress in Photovoltaics : Research and Applications, vol. 16, iss. 8, pp 669-677, Sep 2008.

[59] Takumi Takashima, Junji Yamaguchi, Kenji Otani, Takashi Oozeki, Kazuhiko Kato, Masayoshi Ishida, "Experimental studies of fault location in PV module strings", Solar Energy Materials and Solar Cells, Vol. 93, Iss. 6-7, 17th International Photovoltaic Science and Engineering Conference, June 2009, pp 1079-1082.

[60] J. Johnson, B. Pahl, C.J. Luebke, T. Pier, T. Miller, J. Strauch, S. Kuszmaul, and W. Bower, Photovoltaic DC arc fault detector testing at Sandia National Laboratories, 37th Photovoltaic Specialists Conference, Seattle, WA, June 19-24, 2011.

[61] H. Haeberlin, Arc Detector as an External Accessory Device for PV Inverters for Remote Detection of Dangerous Arcs on the DC Side of PV Plants, European Photovoltaic Solar Energy Conference Valencia, Spain 2010.

[62] J. Johnson, ―Overview of Arc-Faults and Detection Challenges, Arc Fault Detection and Mitigation Webinar, Solar ABCs, February 8, 2010, http://www.solarabcs.org/about/publications/meeting_presentations_minutes/2011/02/pdfs/Johnson_Presentation.pdf

[63] Johnson, J ; Kuszmaul, S; Bower, W; Strauch "PV Arc Fault Detector Challenges due to Module Frequency Response Variability"; Photovoltaic Module Reliability Workshop; Feb 16-17, 2011; Golden, Colorado.

[64] F. Schimpf, L. Norum;" Possibilities for Prevention of Electrical Arcing in PV-Systems"; 24th European Photovoltaic Solar Energy Conference, 21-25 September 2009, Hamburg, Germany.

[65] Buddha, S.; Braun, H.; Krishnan, V.; Tepedelenlioglu, C.; Spanias, A.; Yeider, T.; Takehara, T.; , "Signal processing for photovoltaic applications," Emerging Signal Processing Applications (ESPA), 2012 IEEE International Conference on , vol., no., pp.115-118, 12-14 Jan. 2012.

[66] Shamseldein, M. Z.; Kazerani, M.; Salama, M.M.A, "An Optimal Total Cross Tied Interconnection for Reducing Mismatch Losses in Photovoltaic Arrays," Sustainable Energy, IEEE Transactions on, in press.

[67] D. Picault, B. Raison, S. Bacha, J. de la Casa, J. Aguilera, Forecasting photovoltaic array power production subject to mismatch losses, Solar Energy, Volume 84, Issue 7, July 2010, Pages 1301-1309.

[68] Yaw-Juen Wang, Po-Chun Hsu, An investigation on partial shading of PV modules with different connection configurations of PV cells, Energy, Volume 36, Issue 5, May 2011, Pages 3069-3078.

[69] Villa, L.F.L.; Picault, D.; Raison, B.; Bacha, S.; Labonne, A.; , "Maximizing the Power Output of Partially Shaded Photovoltaic Plants Through Optimization of the Interconnections Among Its Modules, "Photovoltaics, IEEE Journal of , vol.2, no.2, pp.154-163, April 2012.

[70] C. Delin, "Partial Shade Evaluation of Distributed Power Electronics for Photovoltaic Systems," 38st IEEE Photovoltaic specialists conference and Exhibition, June. 2012, Austin, Texas.

[71] Garcia M, Marroyo L, Lorenzo E, Perez M. “Soiling and other optical losses in solar-tracking PV plants in Navarra”. Progress in Photovoltaics: Research and Applications 2011; 19: 211–217.

[72] M. Z. Shams El-Dein, M. Kazerani, and M. M. A. Salama, "Optimal Reconfiguration of Photovoltaic Arrays to Reduce Partial Shading losses". Sustainable Energy, IEEE Transactions on, in press.

[73] Switches and relays Cost, Canada Newark, viewed in August, 2012, http://canada.newark.com/.

[74] Muneer, W.; Bhattacharya, K.; Canizares, C.A.; , "Large-Scale Solar PV Investment Models, Tools, and Analysis: The Ontario Case," Power Systems, IEEE Transactions on , vol.26, no.4, pp.2547-2555, Nov. 2011

[75] University of Colorado; Electrical, Computer and Energy Engineering Departement; “Renewable Energy Sources and Efficient Electrical Energy Systems” ECEN2060 Course materials, Fall 2012.

[76] Jay Johnson, Chris Oberhauser, Michael Montoya, Armando Fresquez, Sigifredo Gonzalez, and Ash Patel, " Crosstalk Nuisance Trip Testing of Photovoltaic DC Arc-Fault Detectors," 38th IEEE Photovoltaic specialists conference, June 3-8, 2012, Austin, Texas.

[77] Jay Johnson, Michael Montoya, Scott McCalmont, Gil Katzir, Felipe Fuks, Justis Earle, Armando Fresquez, Sigifredo Gonzalez, and Jennifer Granata, " Differentiating Series and Parallel Photovoltaic Arc-Faults," 38th IEEE Photovoltaic specialists conference, June 3-8, 2012, Austin, Texas.

[78] W. T. Jewell, R. Ramakumar, “The effects of moving clouds on electric utilities with dispersed PV generation”. IEEE Transactions on Energy Conversion, Vol EC-2, Issue 4, Dec. 1987.

[79] A. Bouthors, F. Neyret, and S. Lefebvre. Real-time realistic illumination and shading of stratiform clouds. In Eurographics Workshop on Natural Phenomena, pages 41–50, 2006